

Extreme-Scale EV Charging Infrastructure Planning for Last-Mile Delivery Using High-Performance Parallel Computing

Waquar Kaleem^a, Taner Cokyasar^b, Jeffrey Larson^b, Omer Verbas^b, Tanveer Hossain Bhuiyan^c, and Anirudh Subramanyam^a

^aPennsylvania State University, University Park, PA 16802, USA

^bArgonne National Laboratory, 9700 S. Cass Avenue, Lemont, IL, 60439 USA

^cUniversity of Texas at San Antonio, One UTSA Circle, San Antonio, TX 78249, USA

February 10, 2025

Abstract

This paper addresses stochastic charger location and allocation (SCLA) problems under queue congestion for last-mile delivery using electric vehicles (EVs). The objective is to decide where to open charging stations and how many chargers of each type to install, subject to budgetary and waiting-time constraints. We formulate the problem as a mixed-integer non-linear program, where each station–charger pair is modeled as a multiserver queue with stochastic arrivals and service times to capture the notion of waiting in fleet operations. The model is extremely large, with billions of variables and constraints for a typical metropolitan area; and even loading the model in solver memory is difficult, let alone solving it. To address this challenge, we develop a Lagrangian-based dual decomposition framework that decomposes the problem by station and leverages parallelization on high-performance computing systems, where the subproblems are solved by using a cutting plane method and their solutions are collected at the master level. We also develop a three-step rounding heuristic to transform the fractional subproblem solutions into feasible integral solutions. Computational experiments on data from the Chicago metropolitan area with hundreds of thousands of households and thousands of candidate stations show that our approach produces high-quality solutions in cases where existing exact methods cannot even load the model in memory. We also analyze various policy scenarios, demonstrating that combining existing depots with newly built stations under multiagency collaboration substantially reduces costs and congestion. These findings offer a scalable and efficient framework for developing sustainable large-scale EV charging networks.

Keywords: Facility Location, Stochastic Charger Location and Allocation, Capacity Allocation, Charging Station, Electric Vehicles, Queuing Systems, Mixed-Integer Quadratic Programming, Large-Scale Optimization

1 Introduction

The global electric vehicle (EV) market has experienced substantial growth, with the fleet size expanding from 11 million in 2020 to approximately 40 million vehicles in 2023 ([International Energy Agency 2024](#)). EV sales accounted for nearly 18% of total car sales in 2023, with projections indicating continued growth to 17 million units in 2024. By 2030, EVs could represent 35% of global car sales, or even 42% to 58% if all manufacturers meet their electrification targets ([International](#)

Energy Agency 2024). To support this increasing demand, government entities and private organizations worldwide must ensure adequate charging infrastructure. The National Renewable Energy Laboratory study (Wood et al. 2023) provides insights into the scale at which EV infrastructure needs to be built. To support 33 million EVs in the United States by 2030, approximately 28 million charging ports of various levels (fast, moderate, and slow chargers) will be necessary. Studies have shown that a lack of EV infrastructure could hamper the growth of EVs (Dolsak and Prakash 2021).

Our work is particularly motivated by the ongoing transformation of urban last-mile delivery through electric vehicle adoption (FareEye 2024). As e-commerce companies seek sustainable and cost-effective solutions for urban logistics, major carriers are making ambitious commitments to electrification. For example, FedEx has announced plans to convert its entire parcel pickup and delivery fleet to zero-emission electric vehicles by 2040 (FedEx Express 2023). EVs have emerged as an attractive option due to their lower operational costs, reduced maintenance requirements, and significant fuel savings. While this transition promises environmental benefits through reduced carbon emissions and improved air quality, it also presents unique operational challenges. Delivery vehicles require reliable access to charging infrastructure while maintaining delivery schedules and service levels. The stochastic nature of delivery routes, varying package volumes, and time-sensitive operations make it crucial to strategically locate charging stations that can handle peak demand periods without causing significant delays in delivery operations. These considerations are especially critical as businesses increasingly scale their electric delivery fleets to meet growing consumer demand for sustainable delivery options.

The EV charging station location problem is a subset of facility location problems that seeks to optimize the locations of charging stations to minimize various costs, including station opening, charger placement, waiting times, and accessibility (Kchaou-Boujelben 2021). Traditionally, this problem has been modeled assuming deterministic demand for electric vehicles and fixed service times (Davatgari et al. 2024), not necessarily incorporating expected waiting time and queue time in the system. In addition, previous studies have focused mainly on small-scale scenarios (in terms of the number of households, charging stations, and chargers considered), limiting their applicability to the large-scale infrastructure needs projected for the future.

Our paper presents a new approach to the EV charging station location problem by formulating it as a stochastic location model with congestion and immobile servers (SLCIS) (e.g., see Berman and Krass (2019)), which we refer to as the stochastic charger location and allocation problem (SCLA). The SLCIS is a facility location model with random service times in which consumers produce streams of random service demands. This results in congestion, as some incoming demands cannot be immediately addressed and must wait in queue (Hale and Moberg 2003). By regarding EV charging stations as immobile servers and EV arrivals as stochastic demands, we incorporate queuing theory and formulate the problem as a mixed-integer non-linear program (MINLP).

We present two exact formulations for the resulting SCLA model. When we scale the models to meet future EV infrastructure needs, however, we find that these exact formulations become prohibitively large and computationally infeasible. In fact, building the model alone can exceed hardware memory limits and make direct solution attempts impractical. To address these scalability challenges, we develop a Lagrangian dual decomposition framework (Guignard 2003), which decomposes the original problem into station-level subproblems that are then solved in parallel using high-performance computing (HPC). We design a customized cutting-plane method to solve the subproblems in parallel on HPC clusters, which reduces both computation time and memory requirements. In addition, we develop novel rounding heuristics that convert fractional Lagrangian solutions into feasible solutions for the exact model. Our approach yields meaningful solutions for extremely large-scale SCLA problem instances with hundreds of thousands of households and

thousands of candidate stations. To the best of our knowledge, such large problems have never been addressed in the literature. Our specific contributions can be summarized as follows:

- We formulate the SCLA problem as a stochastic location model with congestion and immobile servers (chargers) that captures stochasticity in EV charging demand, charging rates, and queue waiting times, thus constituting a realistic framework for large-scale EV infrastructure planning.
- We propose two exact solution methods for the SCLA problem based on mixed-integer nonlinear programming formulations, both of which incorporate cutting-plane methods to handle the nonlinear waiting time constraints.
- To address the scalability limitations of the exact methods, we design a Lagrangian dual decomposition framework. By decomposing the problem into station-level subproblems and solving them in parallel on HPC clusters, we significantly enhance scalability and computational efficiency for extreme-scale SCLA instances. We also design a three-step rounding heuristic to transform the fractional solutions into feasible integral solutions for the exact formulations.
- We implement and demonstrate the proposed framework in the domain of last-mile e-commerce delivery. Through extensive computational experiments and policy analyses, we show that our approach can handle instances far beyond the capabilities of existing exact methods, providing actionable insights for EV infrastructure planning.

The remainder of this paper is organized as follows. [Section 2](#) reviews the relevant literature, [Section 3](#) presents the problem formulation, [Section 4](#) and [Section 5](#) detail the solution approaches, [Section 6](#) presents findings from our computational experiments, and [Section 7](#) offers concluding remarks.

2 Literature Review

Stochastic location models with congestion and immobile servers have seen significant developments over the past few decades ([Berman and Krass 2019](#)). This section summarizes some key contributions, focusing on queuing systems, objective functions, solution methods, and problem sizes addressed. For a concise overview of the queuing notation used in this paper, see [Stewart \(2009, Chapter 11.1.3\)](#). [Amiri \(1997\)](#) used an $M/M/1$ queuing system within the SLCIS model, with the objective to minimize facility opening, detour, and waiting costs. The author employed Lagrangian relaxation ([Guignard 2003](#)) to solve instances with up to 500 user nodes and 40 potential facilities, reporting average CPU times of up to an hour. In another study, [Wang, Batta, and Rump \(2002\)](#) also utilized an $M/M/1$ system with the objective to minimize the expected traveling and waiting costs. They applied greedy heuristics, tabu search ([Glover and Laguna 1998](#)), and ϵ -optimal branch-and-bound methods to problems with 459 customer nodes and 84 potential facility sites, reporting solution times of roughly 1,000 seconds. [Elhedhli \(2006\)](#) extended the $M/M/1$ model to include server capacity costs and used linearization techniques with piecewise linear approximations to solve instances with 100 households and 20 potential service facilities, reporting solution times of up to ten minutes.

Other studies have developed various reformulations to solve SLCIS models. For example, [Gómez et al. \(2017\)](#) reformulated $M/M/1$ systems as a mixed-integer second-order cone optimization problem, solving instances with up to 200 customer nodes and 30 facility locations in roughly

half an hour. Similarly, [Elhedhli et al. \(2018\)](#) developed an approach for $M/M/1$ systems by reformulating the problem as a mixed-integer quadratic program with fourth-degree polynomial constraints and using Lagrangian relaxation, solving problems with up to 100 customer nodes and 15 facility locations, with service rates as continuous decision variables, in about 2.77 hours. In studies by Ahmadi-Javid and collaborators ([Ahmadi-Javid, Berman, and Hoseinpour 2018](#), [Ahmadi-Javid and Ramshe 2020](#), [Ahmadi-Javid and Hoseinpour 2022](#)), the authors used an $M/G/1$ model and developed linear formulations, valid inequalities, and mixed-integer second-order cone programming reformulations for solving SLCIS models with up to 400 customer nodes and 30 facility locations within a time limit of three hours. Likewise, [Vidyarthi and Jayaswal \(2014\)](#), [Vidyarthi et al. \(2015\)](#) adopted an $M/G/1$ queuing system and used linearization with an exact constraint generation algorithm to solve problems with up to 500 customer nodes and 40 facility locations. [Etebari \(2019\)](#) adopted an $M/M/1/k$ model to maximize system profit, employing column generation and hybrid metaheuristics for problems with up to 105 customer nodes and 42 facility locations, with solution times of roughly two hours.

In the work by [Syam \(2008\)](#), the author employed linearization techniques followed by Lagrangian methods ([Guignard 2003](#)) for problems with up to 250 districts and 60 facilities, achieving average solution times of about three minutes. Similarly, [Aboolian, Berman, and Drezner \(2008\)](#) and [Aboolian et al. \(2009\)](#) used an $M/M/s$ system, proposing descent heuristics, simulated annealing, and an exact iterative method consisting of solving an uncapacitated facility location problem. They addressed larger instances with up to 800 customer nodes and 167 potential facility locations, with solution times reaching up to 16 hours. [Castillo, Ingolfsson, and Sim \(2009\)](#) utilized asymptotic approximations for $M/M/s$ systems, originally provided by [Halfin and Whitt \(1981\)](#) and later extended by [Borst, Mandelbaum, and Reiman \(2004\)](#). The authors applied their model to a case study in Edmonton, Canada, considering 38 facility locations and 222 centroids of household neighborhoods. Their work demonstrated that multiserver facilities could be modeled and solved without increased computational effort compared with single-server facilities. [Aboolian, Elhedhli, and Karimi \(2022\)](#) revisited the $M/M/1$ model, comparing several approaches including generalized Benders decomposition. They addressed problems with roughly 100 customer nodes and facility locations and 10 service capacity levels, with solution times up to two hours.

This body of research demonstrates the evolution of solution methods applied to SLCIS, where queuing systems have been modeled by using $M/M/1$, $M/G/1$, and $M/M/s$ models. These models have been applied to diverse settings such as ATM facilities, hospitals, and other service systems. Solution methods have progressed from heuristics to mathematical programming techniques that have enabled solving instances with up to a few hundred households and potential locations.

Numerous studies have explored the optimal placement of electric vehicle charging stations, often relying on various optimization methods ([Kchaou-Boujelben 2021](#)). For instance, [Luo and Qiu \(2020\)](#) used the maximal covering location problem combined with queuing theory to enhance resource utilization of charging stations in sustainable cities. In contrast, [Chen et al. \(2020\)](#) proposed a bilevel mathematical model designed to determine station locations while minimizing construction costs and driver waiting times. In a related effort, [Cui, Weng, and Tan \(2019\)](#) formulated a mixed-integer nonlinear program to minimize the cost of charging stations, network expansion, voltage regulation, and protection device upgrades, thereby catering to urban EV demands. [Erdoğan et al. \(2022\)](#) built on this work by introducing an optimization-based framework that locates fast charging stations along designated corridors. Additional works have accounted for the inherent stochasticity in the system. [Davidov and Pantoš \(2017\)](#) developed a stochastic optimization model that incorporates drivers' uncertain travel patterns, vehicles' driving ranges, and infrastructure service quality. [Xi, Sioshansi, and Marano \(2013\)](#) focused on maximizing the usage of existing charging facilities in central Ohio through a simulation-optimization procedure. [Jordán et al. \(2022\)](#) similarly employed

a simulation-optimization approach, augmented by a genetic algorithm, to pinpoint ideal station locations and then examined how these solutions affect overall EV waiting times and charging station utilization.

Building on this existing body of work, the present paper applies SLCIS methodologies to the placement of electric vehicle charging stations and the allocation of chargers in last-mile delivery settings. Our approach adopts an $M/M/s$ system for this application, an area not yet explored in this context. Notably, and in contrast to existing literature, we design new solution methods that can handle extremely large-scale instances, including hundreds of thousands of households and thousands of potential facilities with varying server configurations. The ability to solve such large-scale problems is key to enabling strategic decision-making in last-mile delivery, where charger placement can have critical long-term impacts on EV adoption and sustainability.

3 Model Description

Consider a graph $(\mathcal{V}, \mathcal{E})$, where \mathcal{V} represents a set of nodes and \mathcal{E} represents edges between nodes. Let $\mathcal{I} \subset \mathcal{V}$ be a discrete set of households, let $\mathcal{J} \subset \mathcal{V}$ be a discrete set of candidate locations for charging stations (*stations* for short), and let \mathcal{K} be the set of charger types with various power outputs. The key decision variables are related to location and allocation. Specifically, define y_j to be a binary variable indicating whether a station $j \in \mathcal{J}$ is opened. Also, define s_{jk} to be an integer variable representing the number of chargers of type $k \in \mathcal{K}$ that are installed at station $j \in \mathcal{J}$. Define x_{ijk} to be a binary variable that denotes whether a charger of type $k \in \mathcal{K}$ at station $j \in \mathcal{J}$ is assigned to EVs that need recharging (immediately) before they serve household $i \in \mathcal{I}$. Given the need for a long-term strategic solution, we adopt a stochastic model of delivery operations that we describe in the following subsections.

3.1 Modeling Household Demand

We assume that each household $i \in \mathcal{I}$ demands delivery at a rate of γ_i per unit time. Given some time interval t (e.g., one week), we may thus interpret $\gamma_i t$ as the average number of times household $i \in \mathcal{I}$ is visited by a delivery vehicle in that time interval. We assume that the demands follow Poisson processes with rates γ_i and that they are independent across households. One can also parameterize γ_i on temporal features such as day of the week or season, in an attempt to reflect household consumption patterns. For simplicity, we do not consider such dependencies, since historical data suggests that over a strategic planning horizon spanning several months to years, the average demand rates of households can be assumed roughly constant.

Let π_i denote the probability of a charging activity occurring immediately before the delivery to household $i \in \mathcal{I}$. The average number of charging activities on the route to household i and the average number of deliveries on the route to household i are denoted by N_i^C and N_i^D , respectively. These parameters can be derived from historical delivery data. The parameter N_i^D can be obtained directly from conventional vehicle routes. Meanwhile, N_i^C can be approximated by dividing each route into segments according to an assumed EV range. In the absence of detailed state-of-charge (SOC) information for the EVs, the probability π_i can be estimated as $\frac{N_i^C}{N_i^D}$. Let $\lambda_i = \gamma_i \pi_i$ denote the charging rate (also referred to as *arrival rate*) for the vehicle delivering to household i . Since γ_i follows a Poisson process and π_i is estimated from historical data, λ_i can also be assumed to follow a Poisson process and to be independent for each household i . Recall that the number of chargers of type $k \in \mathcal{K}$ installed at station $j \in \mathcal{J}$ is denoted as s_{jk} . The charging time of charger type k is assumed to follow an exponential distribution with rate μ_k . In other words, μ_k is the average

number of EVs that can be charged per unit time. The charging service rate μ_k depends on the initial and final SOC for the EVs immediately before and after charging, which we assume to be homogeneous across all vehicles, since the actual vehicle routes—and hence, their SOC—are not known at the time of decision-making.

3.2 Modeling EV Operations

We assume that each household $i \in \mathcal{I}$ is served by an EV that always starts from the depot facility $F_i \in \mathcal{J}$, which is co-located with an existing charging station. This assumption reflects many real-world operations, especially in parcel delivery, where households are preassigned to an existing depot. To reflect actual practice, we assume that if an EV has to recharge immediately before visiting household $i \in \mathcal{I}$, then it can do so only at one of the k_c stations nearest to i . Here, k_c is some predefined parameter that reflects the vehicle’s flexibility, trading off between detouring to nearby but congested stations versus remote but relatively unoccupied stations. To model this flexibility, let subset $\mathcal{J}_i \subseteq \mathcal{J}$ represent the set of feasible stations based on current SOC that an EV can potentially visit immediately before it serves household $i \in \mathcal{I}$, allowing it to charge before delivering to household i . Specifically, we define \mathcal{J}_i as the set of k_c stations that are closest to i with respect to (lat, long) coordinates. Conversely, we also define the subset of households $\mathcal{I}_j \subseteq \mathcal{I}$ that could be visited after charging at a particular station $j \in \mathcal{J}$. More precisely, \mathcal{I}_j is the set of households for which j is among their k_c nearest stations. In other words, $\mathcal{I}_j = \{i \in \mathcal{I} : j \in \mathcal{J}_i\}$.

The sets \mathcal{J}_i and \mathcal{I}_j are crucial to limit the feasible options for each household and station, respectively. This approach replaces the commonly adopted *coverage constraints* (Berman and Krass 2019, Ch. 17, p. 486), eliminating the need for additional constraints to restrict the stations that could be visited prior to each household. Considering all stations as potential charging locations prior to servicing i would not only explode the problem size but also be unrealistic, as the SOC may not allow visiting any given station in the network. Constructing the sets \mathcal{J}_i and \mathcal{I}_j is explained in the Appendix as Algorithm 1.

Let T_{ij} denote the travel time from household $i \in \mathcal{I}$ to station $j \in \mathcal{J}$. Assuming the triangle inequality, the EV detour travel time to visit the station $j \in \mathcal{J}_i$ is then defined as $T_{ij}^\delta := T_{F_i j} + T_{j i} - T_{F_i i}$ for all $i \in \mathcal{I}$ and $j \in \mathcal{J}_i$. Given the extreme scale of SCLA instances considered in this paper, in our implementation, we first perform a fast nearest-neighbor search using a two-dimensional k -d tree on (latitude, longitude) coordinates to select the k_c nearest stations and then compute T_{ij}^δ only for that subset. We note that T_{ij}^δ serves only as an approximation to the true detour travel time, which is difficult to calculate when routes are unknown. Indeed, during actual operations, a vehicle routing problem will be solved to determine the actual delivery sequences, and each EV will charge as needed before delivering to the next household on the route, allowing more precise calculation of the detour time (Davatgari et al. 2024). However, this precise calculation is not possible in our strategic model, since the actual vehicle routes will vary significantly from day to day because of the stochastic nature of household delivery demand, operational uncertainties in travel times, driver availability, and vehicle breakdowns (besides others). We instead adopt a simplified yet realistic model. Crucially, historical delivery and network data can be used to readily inform the parameters of our model, even in the absence of predetermined vehicle routes.

3.3 Modeling Congestion

In extended Kendall’s notation (Stewart 2009, Chapter 11.1.3), we model the queue at each charger type k at station j as an $M/M/s_{jk}/\infty/\infty/\text{FCFS}$ system, where the first M denotes a Poisson arrival process and the second M denotes exponentially distributed service times. This effectively means

that the processes of EV arrivals for recharging and the subsequent service provided by chargers are memoryless and independent. Recall that the term s_{jk} represents the decision variable representing the number of chargers of type k at station j . Also, the first ∞ represents an infinite-length (i.e., uncapacitated) queue, and the second ∞ indicates an infinite population (i.e., very large EV demand at each station-charger pair). *FCFS* indicates a first-come-first-served queuing policy.

Our assumptions imply that EVs form a single queue, waiting to be recharged by all chargers of type k at station j . The expected waiting time, which we denote as \mathbb{W} , includes the queuing and charging times at charger type k at station j . For practical and system efficiency purposes, we impose a prespecified upper bound of EW on \mathbb{W} , reflecting a maximum acceptable limit on the expected waiting time.

Let $\bar{\lambda}_{jk}$ denote the total (decision-dependent) EV demand rate at charger k of station j . Then, the utilization ρ_{jk} is the fraction of time that the particular station-charger pair is busy, and it is simply the ratio of the total demand rate to the total charging service rate at station j for charger type k :

$$\rho_{jk} = \frac{\bar{\lambda}_{jk}}{s_{jk}\mu_k} = \frac{\sum_{i \in \mathcal{I}_j} \lambda_i x_{ijk}}{s_{jk}\mu_k},$$

where we have exploited the fact that the total demand rate $\bar{\lambda}_{jk}$ at station-charger pair (j, k) can be expressed by using the allocation variables as $\bar{\lambda}_{jk} = \sum_{i \in \mathcal{I}_j} \lambda_i x_{ijk}$. For the queue to be stable, we need to ensure $\rho_{jk} < 1$. By introducing a small safety margin, ϵ , we can linearize the constraint $\rho_{jk} < 1$ as follows: $\mu_k s_{jk} (1 - \epsilon) \geq \sum_{i \in \mathcal{I}_j} \lambda_i x_{ijk}$.

The expected waiting time \mathbb{W} depends on the probability \mathbb{P} that all s_{jk} chargers are busy. Both \mathbb{W} and \mathbb{P} are functions of the utilization ratio ρ_{jk} , the number of chargers (servers) s_{jk} , and the charging service rate μ_k . They both admit closed-form expressions, shown below, which can be derived based on standard textbook arguments (Stewart 2009, Chapter 11.4.1).

$$\mathbb{P}(\rho_{jk}, s_{jk}) = \frac{(\rho_{jk} s_{jk})^{s_{jk}}}{(1 - \rho_{jk}) s_{jk}! (T_1 + T_2)}, \quad (1)$$

$$\mathbb{W}(\rho_{jk}, s_{jk}) = \frac{\mathbb{P}(\rho_{jk}, s_{jk})}{\mu_k s_{jk} (1 - \rho_{jk})} + \frac{1}{\mu_k}, \quad (2)$$

where we have defined

$$T_1 = \frac{(\rho_{jk} s_{jk})^{s_{jk}}}{(1 - \rho_{jk}) s_{jk}!}, \quad T_2 = \sum_{r=0}^{s_{jk}-1} \frac{(\rho_{jk} s_{jk})^r}{r!}.$$

3.4 Modeling Costs and Budget Constraints

We let C_j^ϕ be the fixed cost of opening a station $j \in \mathcal{J}$ per unit time, and we let C_k^ξ be the cost of charging the EV using a particular charger type $k \in \mathcal{K}$ per unit time. The detour travel time cost C^δ represents the cost incurred from extending the route because of the need to charge the EV. We let C^τ denote the charging service cost per unit time.

Additionally, we specify budgets for locating stations and allocating chargers, which we denote as B^ϕ and B^ξ per time unit, respectively. We also let \bar{Y} represent the maximum number of stations that can be activated, and we let \bar{S}_{jk} represent the maximum number of type k chargers that can be allocated to station j .

To express the objective function more compactly, we define the indexing set $\mathcal{M} := \{(i, j, k) \mid j \in \mathcal{J}, i \in \mathcal{I}_j, k \in \mathcal{K}\}$. Then, we can define $f_\phi(y) := \sum_{j \in \mathcal{J}} C_j^\phi y_j$ as the station opening cost, $f_\xi(s) := \sum_{j \in \mathcal{J}} \sum_{k \in \mathcal{K}} C_k^\xi s_{jk}$ as the charger installation cost, $f_\delta(x) := \sum_{(i,j,k) \in \mathcal{M}} \lambda_i C^\delta T_{ij}^\delta x_{ijk}$ as the

detour cost, and $f_\tau(x, W) := \sum_{(i,j,k) \in \mathcal{M}} \lambda_i C^\tau W_{jk} x_{ijk}$ as the congestion (waiting) cost. Therefore, the total objective can be expressed as $f_\phi(y) + f_\xi(s) + f_\delta(x) + f_\tau(x, W)$.

3.5 Final Optimization Model

Given the aforementioned assumptions and definitions, the SCLA problem can now be formulated as the following mixed-integer nonlinear program, which we denote as \mathbb{G} . Table 1 summarizes the key notation that we use in this model.

$$\mathbb{G} : \underset{x, y, W, s}{\text{minimize}} \quad f_\phi(y) + f_\xi(s) + f_\delta(x) + f_\tau(x, W) \quad (3)$$

$$\text{subject to} \quad x_{ijk} \leq y_j \quad \forall j \in \mathcal{J}, i \in \mathcal{I}_j, k \in \mathcal{K} \quad (4)$$

$$\sum_{j \in \mathcal{J}, k \in \mathcal{K}} x_{ijk} = 1 \quad \forall i \in \mathcal{I} \quad (5)$$

$$\mu_k s_{jk} (1 - \epsilon) \geq \sum_{i \in \mathcal{I}_j} \lambda_i x_{ijk} \quad (6)$$

$$\forall j \in \mathcal{J}, \forall k \in \mathcal{K}$$

$$\mathbb{W} \left(\frac{\sum_{i \in \mathcal{I}_j} \lambda_i x_{ijk}}{s_{jk} \mu_k}, s_{jk} \right) \leq W_{jk} \quad (7)$$

$$\forall j \in \mathcal{J}, k \in \mathcal{K}$$

$$W_{jk} \leq EW + \frac{1}{\mu_k} \quad (8)$$

$$\forall j \in \mathcal{J}, k \in \mathcal{K}$$

$$f_\phi(y) + f_\xi(s) \leq B^\phi + B^\xi \quad (9)$$

$$f_\phi(y) \leq B^\phi \quad (10)$$

$$f_\xi(s) \leq B^\xi \quad (11)$$

$$\sum_{j \in \mathcal{J}} y_j \leq \bar{Y} \quad (12)$$

$$s_{jk} \leq \bar{S}_{jk} \quad \forall j \in \mathcal{J}, k \in \mathcal{K} \quad (13)$$

$$s_{jk} \leq \bar{S}_{jk} \sum_{i \in \mathcal{I}_j} x_{ijk} \quad (14)$$

$$\forall j \in \mathcal{J}, k \in \mathcal{K}$$

$$y_j \leq \sum_{k \in \mathcal{K}} s_{jk} \quad \forall j \in \mathcal{J} \quad (15)$$

$$x_{ijk}, y_j \in \{0, 1\} \quad (16)$$

$$\forall j \in \mathcal{J}, i \in \mathcal{I}_j, k \in \mathcal{K}$$

$$s_{jk} \in \mathbb{Z}_{\geq 0} \quad \forall j \in \mathcal{J}, k \in \mathcal{K} \quad (17)$$

$$W_{jk} \in \mathbb{R}_{\geq 0} \quad \forall j \in \mathcal{J}, k \in \mathcal{K} \quad (18)$$

The objective function (3) in \mathbb{G} minimizes the total costs for station opening, charger, detour, and congestion (waiting) per time unit. Note that the congestion cost term, $f_\tau(x, W)$, features bilinear products between decision variables, which makes the objective quadratic. Note that W_{jk}

is a dummy variable representing the expected wait time to receive charging service from a charger of type k at station j .

Constraints (4) ensure that charger k at station j cannot be visited by the vehicle serving i unless station j is opened. Constraints (5) enforce that vehicles serving each household must be charged by exactly one charger of some type k at some station j . Constraints (6)–(8) are related to queue congestion and are based on the equations derived in Section 3.3. Specifically, Constraints (6) ensure that the queue stability condition $\rho_{jk} < 1$ is satisfied, that is, the service rate per charger type is strictly greater than its total charging demand rate. Additionally, Constraints (7) and (8) set a lower bound for the service-inclusive waiting time, based on the function \mathbb{W} , and an upper bound with EW , the maximum acceptable queue waiting time.

Constraints (9)–(11) collectively and individually ensure that the costs of station locations and charger allocations do not exceed their respective budgets. Constraints (12) and (13) limit the number of active stations and the allocation of type k chargers at each station, respectively. Constraints (14) ensure that a charger of type k can be allocated at station j only if at least one household i is assigned to it. Constraints (15) ensure that a station j can be opened only if it has at least one charger assigned of any type. Constraints (16), (17), and (18) define the variable domains.

3.6 Differences with Existing Models

Compared with the model from [Aboolian, Berman, and Drezner \(2008\)](#), [Aboolian, Elhedhli, and Karimi \(2022\)](#), [Berman and Drezner \(2007\)](#), our proposed model \mathbb{G} is more general since we do not constrain each household i to be connected to its closest open station j (i.e., the one with shortest travel time). Instead, we introduce the sets \mathcal{J}_i and \mathcal{I}_j to represent the feasible stations for each household and the feasible households for each station, respectively. Recall that the set \mathcal{J}_i contains the k_c nearest stations to household i based on travel times T_{ij} , while \mathcal{I}_j includes the households for which station j is among their k_c nearest stations. The studies by [Aboolian, Berman, and Drezner \(2008\)](#), [Aboolian, Elhedhli, and Karimi \(2022\)](#) assume that (dropping the charger index k without loss of generality) $x_{ij} = 1$ for the household i that is closest to a selected station j . With such an approach, the problem complexity is significantly reduced because the optimal solution of all variables can be derived once the open stations are known. In our proposed model \mathbb{G} , even if we were to fix the open stations (i.e., by fixing the values of the y_j variables), we cannot infer the optimal solution to x_{ijk} for that specific subset of \mathcal{J} . The reason is that the model selects the optimal values of the x_{ijk} (i.e., allocation) decisions not only based on the travel time or the detour travel time between i and j but also considering the queue congestion and the particular charger k used. Moreover, the use of \mathcal{J}_i and \mathcal{I}_j sets in model \mathbb{G} limits the feasible options for each household and station, respectively, replacing the commonly adopted coverage constraints as explained earlier. For these reasons, the exact solutions from [Aboolian, Berman, and Drezner \(2008\)](#), [Aboolian, Elhedhli, and Karimi \(2022\)](#) may not be feasible in our proposed model.

4 Exact Solution Method

In this section, we present an exact solution method for the SCLA model. The method consists of several components, including: a valid inequality ([Section 4.1](#)), a binary representation of the number of chargers s_{jk} ([Section 4.2](#)), linearization of the quadratic objective function ([Section 4.3](#)), and most notably, a cutting plane method for handling the nonlinear waiting time constraints ([Section 4.4](#)), two exact formulations that capture all of these features ([Section 4.5](#)). We conclude

Table 1: Sets, parameters, variables, and cost functions used in model \mathbb{G} .

Set	Definition
\mathcal{V}, \mathcal{E}	vertex set and edge set in the graph representation of the road network.
\mathcal{I}	set of households
\mathcal{I}_j	subset of households that could be visited followed by charging at station $j \in \mathcal{J}$
\mathcal{J}	set of <i>candidate</i> charging stations
\mathcal{J}_i	subset of charging stations that could be visited before serving household $i \in \mathcal{I}$
\mathcal{K}	set of charger types
Parameter	Definition
ϵ	an infinitesimal number
λ_i	charging demand rate (arrival rate) for the vehicle delivering to household $i \in \mathcal{I}$, $\lambda_i = \gamma_i \pi_i$
γ_i	delivery rate to household $i \in \mathcal{I}$
π_i	probability of a charging activity occurring before the delivery to household $i \in \mathcal{I}$, estimated as $\pi_i = \frac{N_i^C}{N_i^D}$, where N_i^C and N_i^D are the number of charging activities on the route to household i and the number of deliveries on the route to household i , respectively
μ_k	service rate of charger type $k \in \mathcal{K}$
T_{ij}	travel time from $i \in \mathcal{I}$ to $j \in \mathcal{J}$
T_{ij}^δ	detour travel time when station $j \in \mathcal{J}_i$ is visited immediately before serving household $i \in \mathcal{I}$
C^δ	cost of detour per time unit
C^τ	cost of wait time and service time per time unit
C_j^ϕ	fixed cost of charging station $j \in \mathcal{J}$ per time unit
C_k^ξ	cost of installing a type k charger per time unit
Variable	Definition
ρ_{jk}	utilization rate of charger type k at station j , $\rho_{jk} \in \mathbb{R}_{\geq 0}$, $\rho_{jk} < 1$, $\rho_{jk} = \frac{\sum_{i \in \mathcal{I}_j} (\lambda_i x_{ijk})}{\mu_k s_{jk}}$
s_{jk}	number of type k chargers allocated to station $j \in \mathcal{J}$, $s_{jk} \in \mathbb{Z}_{\geq 0}$
W_{jk}	expected waiting (including charging) time for charger type $k \in \mathcal{K}$ at station $j \in \mathcal{J}$, $W_{jk} \in \mathbb{R}_{\geq 0}$
x_{ijk}	$\begin{cases} 1 & \text{if charger type } k \in \mathcal{K} \text{ at station } j \in \mathcal{J}_i \text{ is visited to charge the vehicle} \\ & \text{preceding household } i \in \mathcal{I} \\ 0 & \text{otherwise} \end{cases}$
y_j	$\begin{cases} 1 & \text{if station } j \in \mathcal{J} \text{ is active} \\ 0 & \text{otherwise} \end{cases}$
Cost Functions	Definition
$f_\phi(y)$	station opening cost: $f_\phi(y) = \sum_{j \in \mathcal{J}} C_j^\phi y_j$
$f_\xi(s)$	charger installation cost: $f_\xi(s) = \sum_{j \in \mathcal{J}} \sum_{k \in \mathcal{K}} C_k^\xi s_{jk}$
$f_\delta(x)$	detour cost: $f_\delta(x) = \sum_{(i,j,k) \in \mathcal{M}} \lambda_i C^\delta T_{ij}^\delta x_{ijk}$
$f_\tau(x, W)$	congestion (waiting) cost: $f_\tau(x, W) = \sum_{(i,j,k) \in \mathcal{M}} \lambda_i C^\tau W_{jk} x_{ijk}$

this section by presenting computational challenges of the exact formulation for extreme-scale problems (Section 4.6).

4.1 A Valid Inequality

Recall that for each station $j \in \mathcal{J}$, \mathcal{I}_j is the set of households that can potentially be assigned to j . The household $i \in \mathcal{I}_j$ cannot be assigned to more than one charger type $k \in \mathcal{K}$ at station j . This constraint can be expressed by the inequality $\sum_{k \in \mathcal{K}} x_{ijk} \leq 1$ for all $i \in \mathcal{I}_j$. Imposing these inequalities for each station j strengthens formulation \mathbb{G} without cutting off any of its integer feasible solutions. The following theorem formally proves this claim.

Theorem 1. *For any $j \in \mathcal{J}$, the inequality $\sum_{k \in \mathcal{K}} x_{ijk} \leq 1$ for all $i \in \mathcal{I}_j$ is valid for model \mathbb{G} .*

Proof. Proof: Assume for contradiction that there exist $j \in \mathcal{J}$ and $i \in \mathcal{I}_j$ such that $\sum_{k \in \mathcal{K}} x_{ijk} > 1$. The set partitioning constraint, $\sum_{j' \in \mathcal{J}, k \in \mathcal{K}} x_{ij'k} = 1$, ensures that household i is assigned to exactly one station-charger pair in the entire network. Now, since $\sum_{k \in \mathcal{K}} x_{ijk} > 1$ at station j , then i must be assigned to multiple chargers at the same station, violating the uniqueness imposed by the set partitioning constraint. This contradiction implies that no feasible integral solution can violate the inequality. \square

4.2 Binary Representation of the Number of Chargers

To handle the discrete nature of charger allocation, we introduce a binary representation that allows us to precisely model the number of chargers at each station. To that end, define the set $\mathcal{S} = \{0, 1, 2, \dots, \max_{j \in \mathcal{J}, k \in \mathcal{K}} \bar{S}_{jk}\}$, which represents all possible discrete numbers of chargers that can be allocated at station j for each charger type k . We then introduce the binary variable z_{cjk} to indicate whether $c \in \mathcal{S}$ number of type k chargers are allocated to station j . In the following, we present model \mathbb{G} with the incorporation of the valid inequality from the previous section and the binarization of charger allocations.

$$\begin{aligned} \min_{x, y, W, s, z} \quad & f_\phi(y) + f_\xi(s) + f_\delta(x) + f_\tau(x, W) \\ \text{s. t.} \quad & (4) - (18) \\ & \sum_{k \in \mathcal{K}} x_{ijk} \leq 1 \quad \forall j \in \mathcal{J}, i \in \mathcal{I}_j \end{aligned} \tag{19}$$

$$s_{jk} = \sum_{c \in \mathcal{S}} c \cdot z_{cjk} \quad \forall j \in \mathcal{J}, k \in \mathcal{K} \tag{20}$$

$$\sum_{c \in \mathcal{S}} z_{cjk} \leq y_j \quad \forall j \in \mathcal{J}, k \in \mathcal{K} \tag{21}$$

$$z_{cjk} \in \{0, 1\} \quad \forall c \in \mathcal{S}, j \in \mathcal{J}, k \in \mathcal{K}. \tag{22}$$

The constraints (19) ensure that given a station j , each household is assigned to at most one charger type. Constraints (20) link the number of chargers s_{jk} to the binary variables z_{cjk} , ensuring that the correct number of chargers are allocated. Constraints (21) ensure that chargers are allocated only if the station is open.

4.3 Linearizing the Objective Function

The bilinear term $W_{jk}x_{ijk}$ in the objective function term, $f_\tau(x, W)$, makes the solution of the model computationally challenging. To address the bilinear terms, we explore the use of McCormick inequalities (McCormick 1976). Consider linearizing $q_{ijk} = W_{jk}x_{ijk}$ over the domain $\mathcal{B} = [0, EW + 1/\mu_k] \times \{0, 1\}$. Recall that $W_{jk} \in [0, EW + 1/\mu_k]$ is the expected waiting time including charging time and $x_{ijk} \in \{0, 1\}$ is a binary variable. It is well known that the convex hull of the set $\{(W_{jk}, x_{ijk}, q_{ijk}) \in (\mathcal{B} \times \mathbb{R}) \mid q_{ijk} = W_{jk}x_{ijk}\}$ can be described using the following inequalities:

$$\begin{aligned} q_{ijk} &\geq 0, \\ q_{ijk} &\geq W_{jk} - \left(EW + \frac{1}{\mu_k}\right)(1 - x_{ijk}), \\ q_{ijk} &\leq \left(EW + \frac{1}{\mu_k}\right)x_{ijk}, \\ q_{ijk} &\leq W_{jk}. \end{aligned} \tag{23}$$

This set of inequalities (23), also known as the McCormick inequalities, defines the convex and concave envelopes of $W_{jk}x_{ijk}$ on the domain \mathcal{B} . Specifically, the first inequality ensures non-negativity of q_{ijk} . The second inequality ensures $q_{ijk} \geq W_{jk}$ when $x_{ijk} = 1$, whereas the third inequality ensures $q_{ijk} = 0$ when $x_{ijk} = 0$. The fourth inequality ensures q_{ijk} never exceeds W_{jk} . We note that these inequalities provide an exact linearization of the bilinear term, since x_{ijk} is binary. Therefore, we can equivalently rewrite the objective by replacing $W_{jk}x_{ijk}$ with q_{ijk} , resulting in:

$$\begin{aligned} \min_{x, y, W, s, z, q} \quad & f_\phi(y) + f_\xi(s) + f_\delta(x) + \sum_{(i, j, k) \in \mathcal{M}} \lambda_i C^\tau q_{ijk} \\ \text{s.t.} \quad & (4) - (23), \end{aligned} \tag{24}$$

where it is understood that the McCormick inequalities (23) are written for all $(i, j, k) \in \mathcal{M}$.

4.4 Cutting-Plane Approach for Nonlinear Constraints

We now address the nonlinearity arising from the expected waiting time function \mathbb{W} . We employ a cutting-plane approach that iteratively approximates \mathbb{W} by introducing valid linear inequalities. The expected waiting time function, $\mathbb{W}(\rho_{jk}, s_{jk})$, which models an $M/M/s_{jk}$ queue, exhibits fundamental characteristics derived from the Erlang delay formula. Prior results (Grassmann 1983, Lee and Cohen 1983) establish that \mathbb{W} is strictly increasing and strictly convex with respect to its first argument, the utilization ratio ρ_{jk} , whenever the stability condition $0 < \rho_{jk} < 1$ is satisfied.

Property 1. *For all $s_{jk} \in \mathbb{Z}_{>0}$, the function $\mathbb{W}(\cdot, s_{jk})$ is strictly increasing and strictly convex over the domain $(0, 1)$.*

We can exploit Property 1 to design a Kelley-type cutting plane method (Kelley 1960, Cokyasar and Jin 2023) to handle the nonlinear waiting time constraints. These constraints iteratively enforce lower bounds on \mathbb{W} by adding supporting hyperplanes as cuts. To see this, temporarily fix s_{jk} and observe that Property 1 also applies to the function $\mathbb{W}^\nu(\rho_{jk})$ defined as follows:

$$\mathbb{W}^\nu(\rho_{jk}) = \frac{\mathbb{P}(\rho_{jk}, s_{jk})}{1 - \rho_{jk}} \tag{25}$$

For any fixed candidate value $0 < \tilde{\rho}_{jk} < 1$, define

$$B_{jk} = \frac{\partial \mathbb{W}^\nu}{\partial \rho_{jk}}(\tilde{\rho}_{jk}), \quad A_{jk} = \mathbb{W}^\nu(\tilde{\rho}_{jk}) - B_{jk}\tilde{\rho}_{jk}.$$

Then, [Property 1](#) implies that the line, $A_{jk} + B_{jk}\rho_{jk}$, supports the graph of the function, $\mathbb{W}^\nu(\rho_{jk})$, at $\rho_{jk} = \tilde{\rho}_{jk}$. This implies $W_{jk} \geq (A_{jk} + B_{jk}\rho_{jk})/(\mu_k s_{jk}) + 1/\mu_k$. However, note that this constraint is nonlinear in s_{jk} . To address this nonlinearity, we introduce this constraint only conditionally on the current values of ρ_{jk} and s_{jk} . Enforcing the constraints conditionally will ensure a valid lower bound on \mathbb{W} for all possible values of the decision variables, thus ensuring that they can be added as global cuts within a branch-and-bound search process. The conditional requirement can be imposed by exploiting the binary representation of s_{jk} that we introduced previously. Also, since ρ_{jk} is a function of only s_{jk} and x_{ijk} , the conditional requirements can thus effectively be enforced using the values of only the binary variables z_{cjk} and x_{ijk} , as shown below.

$$\begin{aligned} W_{jk} \geq & \frac{A_{jk}z_{cjk}}{\mu_k c} \\ & + \frac{B_{jk} \sum_{i \in \mathcal{I}_j} \lambda_i (z_{cjk} + x_{ijk} - 1)}{\mu_k^2 c^2} \\ & + \frac{z_{cjk}}{\mu_k} \quad \forall c \in \mathcal{S} \setminus \{0\}, j \in \mathcal{J}, k \in \mathcal{K} \end{aligned} \quad (26)$$

The constraints in equation (26) leverage the binary variable z_{cjk} to establish the relationship between waiting time W_{jk} and the number of allocated chargers. Recall that z_{cjk} indicates whether c chargers of type k are assigned to station j . When $z_{cjk} = 1$, the constraint becomes active for the specific number of chargers c , enforcing a lower bound on the waiting time based on the allocated chargers. On the other hand, when $z_{cjk} = 0$, the constraint becomes slack, allowing the solver to effectively disregard that particular constraint.

In actual implementation, note that we remove the constraint (7) from the original model and instead add the conditional constraints (26) as lazy constraints every time an integer solution is obtained during the branch-and-bound process. Notably, we do not need to add the constraint (26) for all possible values of c , j and k simultaneously. Instead, as the solver progresses and comes up with integer solutions for a specific configuration of chargers for a given j and k , we apply this cut only for the current c at the current node. This approach ensures accurate bounding of W_{jk} based on the actual number of allocated chargers. The binary nature of z_{cjk} along with constraint (21) guarantees that only one constraint is active for each combination of j and k , corresponding to the chosen number of chargers in the current integer solution. Note that when $s_{jk} = 0$, the constraint is undefined and never added.

To measure convergence during the solution process, let \mathbb{C} denote the objective value of the best-known integral feasible solution found so far, and let $\overline{\mathbb{C}}$ be the current best-known upper bound on the optimal objective. Define the solution gap as $Q := 1 - (\mathbb{C}/\overline{\mathbb{C}})$, which quantifies how close the current solution is to optimality.

The branch-and-bound procedure starts off by solving the SCLA problem formulation without constraint (7). Each time we encounter a feasible MIP node satisfying all other constraints including integrality constraints, we enter a solver callback, that uses the solution vectors \mathbf{s} , \mathbf{x} , and \mathbf{y} to calculate (i) $\tilde{\rho}_{jk} = \sum_{i \in \mathcal{I}_j} \lambda_i x_{ijk} / (\mu_k s_{jk})$; (ii) \overline{W}_{jk} , the upper bound (value) of W_{jk} via $\tilde{\rho}_{jk}$; (iii) $\overline{\mathbb{C}}$, the upper bound (value) of \mathbb{C} via \overline{W}_{jk} ; and (iv) the solution gap $Q := 1 - (\mathbb{C}/\overline{\mathbb{C}})$. While $Q > Q^\tau$, where Q^τ is an acceptable gap threshold, we use s_{jk} as calculated from the binary variables and introduce (7) to j and k only when $s_{jk} > 0$ and $W_{jk} < \overline{W}_{jk}$. Therefore, constraints (7) are

introduced only for specific charger types at stations where (i) at least one charger is allocated and (ii) the value of W_{jk} is underestimated. When the condition $Q \leq Q^\tau$ is met or a predefined solution time limit is reached, the solver terminates and reports the best solution found.

4.5 Summary of Exact Formulations

After replacing constraint (7) with constraint (26), we obtain two exact formulations for the SCLA problem. The mixed-integer quadratic program (MIQP) is denoted as E_{MIQP} and shown below.

$$\begin{aligned} \min_{x,y,W,s,z} \quad & f_\phi(y) + f_\xi(s) + f_\delta(x) + f_\tau(x, W) \\ \text{s.t.} \quad & (4) - (6), (8) - (22), (26) \end{aligned}$$

The mixed-integer linear program (MILP) is denoted E_{MCC} and shown below.

$$\begin{aligned} \min_{x,y,W,s,z,q} \quad & (24) \\ \text{s.t.} \quad & (4) - (6), (8) - (23), (26) \end{aligned}$$

4.6 Computational Challenges

Our primary aim in this paper is to solve extremely large-scale instances of the SCLA problem, encompassing an immense number of households, candidate stations, and charger types. Even with a carefully formulated MIQP or MILP model, the dimensionality of the problem escalates rapidly. As $|\mathcal{I}|$, $|\mathcal{J}|$, and $|\mathcal{K}|$ grow large, the indexing set $\mathcal{M} := \{(i, j, k) \mid j \in \mathcal{J}, i \in \mathcal{I}_j, k \in \mathcal{K}\}$ can contain an enormous number of elements. Each such (i, j, k) triplet requires a binary assignment variable $x_{ijk} \in \{0, 1\}$, and every station-charger pair (j, k) may demand multiple binary configuration variables $z_{cjk} \in \{0, 1\}$ indexed by $c \in \mathcal{S}$. The result is a model with a massive number of binary variables, supplemented by integer charger allocation variables s_{jk} and continuous waiting time variables W_{jk} , among others. When McCormick linearizations are applied in the E_{MCC} formulation, each bilinear term $W_{jk}x_{ijk}$ is replaced by a continuous variable q_{ijk} and multiple additional constraints. This further inflates the number of variables and constraints, pushing the limits of memory and computational time. Coupled with the complex nonlinear constraints related to the queuing-based expected waiting times, the resulting MIQP or MILP is extraordinarily challenging for commercial solvers. Constructing, loading, and solving such a colossal formulation directly are impractical; and obtaining high-quality solutions within a reasonable timeframe is effectively impossible. These computational challenges necessitate an alternative approach that exploits problem structure, reduces overhead, and can be parallelized. In the following sections, we propose a decomposition framework based on Lagrangian relaxation, designed to handle extreme-scale SCLA instances efficiently and reliably.

5 A Lagrangian-Based Decomposition Framework

Our proposed solution approach for the SCLA problem integrates multiple components. We begin by applying Lagrangian relaxation (Section 5.1) to introduce dual variables associated with key constraints. Building on this, we employ Lagrangian dual decomposition (Section 5.2) to decompose the relaxed problem into station-level subproblems, each of which can be solved independently and in parallel. To solve each station-level subproblem, we employ a partial relaxation strategy combined with cutting-plane methods (Section 5.3). We iteratively update the Lagrange multipliers via a subgradient method (Section 5.4). We then apply a three step rounding heuristic (Section 5.5)

to convert the fractional assignments from the subproblems into a feasible integral solution for the entire SCLA problem. Together, these techniques produce an integrated, scalable, and effective framework capable of handling large-scale SCLA problem instances.

5.1 Lagrangian Relaxation

Observe that the set partitioning constraint (5) and the budget constraints (9)–(12) are complicating constraints in formulation \mathbb{G} : the latter completely decomposes into smaller and independent subproblems, in the absence of these constraints. To exploit this structure, we introduce a Lagrange multiplier ζ_i for each equality constraint (5), corresponding to household i . To ensure non-negativity of these multipliers, we first modify the equality constraint (5) to a set covering constraint: $\sum_{j \in \mathcal{J}, k \in \mathcal{K}} x_{ijk} \geq 1 \quad \forall i \in \mathcal{I}$. This is without loss of generality, since doing so does not change the optimal solution of model \mathbb{G} . However, ζ_i can now only take non-negative values ($\zeta_i \geq 0$). Similarly, we also introduce multipliers θ , β_ϕ , β_ξ , and ν corresponding to the total budget constraint (9), the station budget constraint (10), the charger budget constraint (11), and the limit on the number of active stations (12). The resulting Lagrangian relaxation, $L(\zeta, \theta, \beta_\phi, \beta_\xi, \nu)$, of model \mathbb{G} is given by:

$$\begin{aligned}
\min_{x, y, W, s, z} \quad & f_\phi(y) + f_\xi(s) + f_\delta(x) + f_\tau(x, W) \\
& + \sum_{i \in \mathcal{I}} \zeta_i \left(1 - \sum_{j \in \mathcal{J}, k \in \mathcal{K}} x_{ijk} \right) \\
& + \theta (f_\phi(y) + f_\xi(s)) - \theta (B^\phi + B^\xi) \\
& + \beta_\phi (f_\phi(y) - B^\phi) + \beta_\xi (f_\xi(s) - B^\xi) \\
& + \nu \left(\sum_{j \in \mathcal{J}} y_j - \bar{Y} \right) \\
\text{s. t.} \quad & (4), (6) - (8), (13) - (22).
\end{aligned} \tag{27}$$

5.2 Lagrangian Dual and Decomposition

The Lagrangian dual D of model \mathbb{G} , seeks the tightest lower bound on the optimal value of \mathbb{G} . Formally, if $L(\zeta, \theta, \beta_\phi, \beta_\xi, \nu)$ denotes the optimal objective value of the Lagrangian relaxation corresponding to fixed multipliers $(\zeta, \theta, \beta_\phi, \beta_\xi, \nu)$, then the dual problem D can be defined as:

$$D = \max_{\zeta, \theta, \beta_\phi, \beta_\xi, \nu \geq 0} L(\zeta, \theta, \beta_\phi, \beta_\xi, \nu).$$

To demonstrate the decomposition arising in the inner minimization, we use the extensive form notation from Table 1. In this form, the Lagrangian separates by station index j , leading to independent station-level subproblems $SP_j(\zeta, \theta, \beta_\phi, \beta_\xi, \nu)$. Formally, we have:

$$\begin{aligned}
L(\zeta, \theta, \beta_\phi, \beta_\xi, \nu) = \quad & \sum_{j \in \mathcal{J}} SP_j(\zeta, \theta, \beta_\phi, \beta_\xi, \nu) \\
& + \sum_{i \in \mathcal{I}} \zeta_i - \theta (B^\phi + B^\xi) \\
& - \beta_\phi B^\phi - \beta_\xi B^\xi - \nu \bar{Y}.
\end{aligned} \tag{28}$$

Because the Lagrangian function is separable by station index j , the minimization problem splits into independent subproblems $SP_j(\zeta, \theta, \beta_\phi, \beta_\xi, \nu)$, each involving only the variables and parameters associated with that station. This decomposition allows for the concurrent solution of all SP_j and efficient handling of extremely large-scale instances. For each fixed station $j \in \mathcal{J}$, the subproblem (SP_j) can be stated as follows:

$$\begin{aligned} \min_{x,y,W,s,z} & [(1 + \theta + \beta_\phi)C_j^\phi + \nu]y_j \\ & + \sum_{k \in \mathcal{K}} [(1 + \theta + \beta_\xi)C_k^\xi]s_{jk} \\ & + \sum_{i \in \mathcal{I}} \sum_{k \in \mathcal{K}} (C^\delta T_{ij}^\delta \lambda_i + C^\tau W_{jk} \lambda_i - \zeta_i)x_{ijk} \end{aligned} \quad (29)$$

$$\text{s. t. } x_{ijk} \leq y_j \quad \forall i \in \mathcal{I}_j, k \in \mathcal{K} \quad (30)$$

$$\sum_{k \in \mathcal{K}} x_{ijk} \leq 1 \quad \forall i \in \mathcal{I}_j \quad (31)$$

$$\mu_k s_{jk}(1 - \epsilon) \geq \sum_{i \in \mathcal{I}_j} \lambda_i x_{ijk} \quad \forall k \in \mathcal{K} \quad (32)$$

$$\mathbb{W} \left(\frac{\sum_{i \in \mathcal{I}_j} \lambda_i x_{ijk}}{s_{jk} \mu_k}, s_{jk} \right) \leq W_{jk} \quad \forall k \in \mathcal{K} \quad (33)$$

$$W_{jk} \leq EW + \frac{1}{\mu_k} \quad \forall k \in \mathcal{K} \quad (34)$$

$$s_{jk} \leq \bar{S}_{jk} \quad \forall k \in \mathcal{K} \quad (35)$$

$$s_{j,k} \leq \bar{S}_{jk} \sum_{i \in \mathcal{I}_j} x_{ijk} \quad \forall k \in \mathcal{K} \quad (36)$$

$$y_j \leq \sum_{k \in \mathcal{K}} s_{jk} \quad (37)$$

$$s_{jk} = \sum_{c \in \mathcal{S}} c \cdot z_{cjk} \quad k \in \mathcal{K} \quad (38)$$

$$\sum_{c \in \mathcal{S}} z_{cjk} \leq y_j \quad \forall k \in \mathcal{K} \quad (39)$$

$$z_{cjk} \in \{0, 1\} \quad \forall c \in \mathcal{S}, k \in \mathcal{K} \quad (40)$$

$$x_{ijk}, y_j \in \{0, 1\} \quad \forall i \in \mathcal{I}_j, k \in \mathcal{K} \quad (41)$$

$$s_{jk} \in \mathbb{Z}_{\geq 0}, \quad W_{jk} \in \mathbb{R}_{\geq 0} \quad \forall k \in \mathcal{K}. \quad (42)$$

Each station-level subproblem SP_j focuses on station opening, charger installation, detour costs, and waiting times for station j only, independent of all other stations. In the next section we present two solution approaches for solving SP_j .

5.3 Partial Linear Relaxation with Cutting Planes

Observe that subproblem SP_j is a simpler version of the full-scale problem, restricted to station j and without any complicating constraints that couple these stations. Therefore, it is possible directly apply the solution method from Section 4 to solve SP_j . However, computational experiments on extremely large-scale instances demonstrate significant hurdles. Even when focusing on a single

station j , the cardinality $|\mathcal{I}_j|$ of the household set and the associated binary decision variables x_{ijk} can be exceptionally large. As a result, the decomposed subproblems also become computationally intractable, exceeding practical time limits.

To address this challenge, we present modified variants of the exact methods, E_{MIQP} and E_{MCC} , for the Lagrangian subproblems SP_j . These variants, denoted as L_{MIQP} and L_{MCC} , are similar to their exact counterparts. The only modification is the relaxation of integrality conditions on the binary variables x_{ijk} . As a consequence, they only constitute relaxations of SP_j . Although these relaxations simplify the subproblem and reduce computational complexity, it is important to note that they continue to provide rigorous lower bounds on the optimal value of the original SCLA problem. However, at the same time, they may also yield fractional solutions that are not integer-valued. To regain integer feasibility, we develop specialized rounding heuristics that transform the fractional solutions into integral ones.

5.3.1 L_{MIQP} Formulation for Solving SP_j .

We relax $x_{ijk} \in [0, 1]$. Note that the other integer variables, namely y_j , z_{cjk} , and s_{jk} retain their original discrete domains. The objective and constraints remain identical to the problem SP_j defined in equations (29)–(42) except we replace $x_{ijk} \in \{0, 1\}$ with $0 \leq x_{ijk} \leq 1$. The resulting formulation can be summarized as follows.

$$\begin{aligned} \min_{x,y,W,s,z} \quad & (29) \\ \text{s.t.} \quad & (30) - (40), (42) \\ & 0 \leq x_{ijk} \leq 1, y_j \in \{0, 1\}. \end{aligned} \quad (43)$$

5.3.2 L_{MCC} Formulation for Solving SP_j .

Similar to L_{MIQP} , the L_{MCC} formulation relaxes $x_{ijk} \in [0, 1]$ in the original E_{MCC} model, whereas y_j , z_{cjk} , and s_{jk} continue to remain discrete. Similarly, the bilinear term $W_{jk}x_{ijk}$ is linearized via an auxiliary variable q_{ijk} and appropriate McCormick-type inequalities. The objective and constraints reflect those of the problem SP_j but with $x_{ijk} \in [0, 1]$ and q_{ijk} introduced to represent the convex hull of the product $W_{jk}x_{ijk}$.

$$\begin{aligned} \min_{x,y,W,s,z,q} \quad & [(1 + \theta + \beta_\phi)C_j^\phi + \nu]y_j \\ & + \sum_{k \in \mathcal{K}} [(1 + \theta + \beta_\xi)C_k^\xi]s_{jk} \\ & + \sum_{i \in \mathcal{I}} \sum_{k \in \mathcal{K}} ((C^\delta T_{ij}^\delta \lambda_i - \zeta_i)x_{ijk} + C^\tau \lambda_i q_{ijk}) \\ \text{s.t.} \quad & (23), (30) - (40), (42), (43) \end{aligned} \quad (44)$$

In both L_{MIQP} and L_{MCC} subproblem formulations, the nonlinear waiting-time constraint (33) is replaced by the cutting-plane constraint (26), applied for each fixed station j .

5.4 Subgradient Method for Updating Lagrangian Multipliers

The subproblems SP_j are solved for fixed values of the Lagrange multipliers ζ , θ , β_ϕ , β_ξ , ν . Aggregating the subproblem solutions allows us to calculate the Lagrangian objective value, $L(\zeta, \theta, \beta_\phi, \beta_\xi, \nu)$,

shown in (28). The Lagrangian dual, which provides a lower bound to the original problem \mathbb{G} , can further be improved by updating the Lagrange multipliers. To that end, we employ the classical subgradient method (Boyd, Xiao, and Mutapcic 2003, Barahona and Chudak 2005, Barahona and Anbil 2000) to update the multipliers, which consist of the following steps.

Step 0: Let $\eta = (\zeta, \theta, \beta_\phi, \beta_\xi, \nu)$ denote the tuple of Lagrange multipliers. Initialize $\eta^0 = 0$. Solve subproblem SP_j for all station locations $j \in \mathcal{J}$, independently and in parallel, to obtain subproblem-optimal solutions $x_{ijk}^0, y_j^0, s_{jk}^0, W_{jk}^0$ for each SP_j . Aggregate these solutions and evaluate the Lagrangian $\mathcal{L}(\eta^0)$. Run a rounding heuristic (Section 5.5) on the aggregated solution to obtain a feasible solution with objective value z^0 , and set the initial upper bound $UB = z^0$. Set $t = 1$, $\lambda_\eta^1 = 0.1$, and $\eta' = \eta^0$.

Step 1: Compute the subgradients for all Lagrange multipliers at iteration t as follows:

$$g_{\zeta_i}^t = 1 - \sum_{j \in \mathcal{J}, k \in \mathcal{K}} x_{ijk}^{t-1} \quad \forall i \in \mathcal{I} \quad (45)$$

$$g_\theta^t = \sum_{j \in \mathcal{J}} C_j^\phi y_j^{t-1} + \sum_{j \in \mathcal{J}, k \in \mathcal{K}} C_k^\xi s_{jk}^{t-1} - (B^\phi + B^\xi) \quad (46)$$

$$g_{\beta_\phi}^t = \sum_{j \in \mathcal{J}} C_j^\phi y_j^{t-1} - B^\phi \quad (47)$$

$$g_{\beta_\xi}^t = \sum_{j \in \mathcal{J}, k \in \mathcal{K}} C_k^\xi s_{jk}^{t-1} - B^\xi \quad (48)$$

$$g_\nu^t = \sum_{j \in \mathcal{J}} y_j^{t-1} - \bar{Y}. \quad (49)$$

Compute step sizes s_η^t for each component $\eta \in \{\{\zeta_i\}_{i \in \mathcal{I}}, \theta, \beta_\phi, \beta_\xi, \nu\}$ as follows:

$$s_\eta^t = \lambda_\eta^t \frac{\Delta}{\|g_\eta^t\|^2}, \text{ where } \Delta = UB - \mathcal{L}(\eta'),$$

UB is any valid upper bound on the optimal objective value of the original formulation \mathbb{G} , η' represents the best multipliers found so far, and $\lambda_\eta^t \in (0, 2)$ is a step length parameter for each η . Using these step sizes, we update the multipliers as follows:

$$\eta^t = \max(0, \eta^{t-1} + s_\eta^t g_\eta^t).$$

This process ensures that each Lagrange multiplier is updated independently, taking into account its specific subgradient and step size.

Step 2: Evaluate $\mathcal{L}(\eta^t)$ by solving SP_j for all station locations $j \in \mathcal{J}$, independently and in parallel, to obtain subproblem-optimal solutions $x_{ijk}^t, y_j^t, s_{jk}^t, W_{jk}^t$ for each SP_j . Run a rounding heuristic (Section 5.5) on the new aggregated solution to obtain a feasible solution with objective value z^t . If $z^t < UB$, update the upper bound by setting $UB \leftarrow z^t$.

Step 3: For each η , update λ_η^t as follows.

- If $\mathcal{L}(\eta^t) \leq \mathcal{L}(\eta')$, then no improvement has been achieved: label the iteration as *red*, indicating that the current step size for η is likely too large. Reduce $\lambda_\eta^t = \frac{9}{10} \lambda_\eta^{t-1}$ to encourage progress in subsequent iterations.
- If $\mathcal{L}(\eta^t) > \mathcal{L}(\eta')$, perform a directional test by forming direction vectors from current (g_η^t) and aggregated (\bar{g}_η^t) subgradients, i.e. let $v_\eta^t = g_\eta^t - \bar{g}_\eta^t$. Then compute the inner product $d_\eta = \langle v_\eta^t, g_\eta^t \rangle$:

- If $d_\eta \geq 0$, label the iteration as *green*, suggesting that even larger steps, $\lambda_\eta^t = 1.1\lambda_\eta^{t-1}$, could yield further improvement.
- If $d_\eta < 0$, label the iteration as *yellow*, indicating that the current step size is roughly appropriate, and we keep $\lambda_\eta^t = \lambda_\eta^{t-1}$ unchanged.

Since each λ_η^t is updated independently based on the multiplier’s own classification, this process systematically refines step sizes, guiding the subgradient method toward improved dual bounds and enhanced solution quality over time.

Step 4: If $\mathcal{L}(\eta^t) > \mathcal{L}(\eta')$, update $\eta' \leftarrow \eta^t$. Go to **Step 1**.

5.5 Rounding Heuristic

The Lagrangian-based decomposition provides lower bounds on the original problem \mathbb{G} , but may not produce primal feasible solutions. To address this issue, we develop a rounding heuristic that uses the station-level solutions from the Lagrangian subproblems SP_j to construct a feasible primal solution obtain an upper bound on \mathbb{G} . We emphasize that the heuristic is not an independent procedure; rather, it is explicitly driven by and dependent on the subproblem solutions $(x_{ijk}^t, y_j^t, s_{jk}^t, W_{jk}^t)$ obtained after solving all subproblems SP_j for every $j \in \mathcal{J}$, in Step 2 of the procedure described in the previous subsection.

The rounding procedure ([Algorithm 6](#)) consists of three main steps, each realized through a set of algorithms that refine the partially relaxed solution into a fully integral one. The procedure begins with the station opening decisions y_j^t and fractional household assignments x_{ijk}^t at iteration t , and produces a final solution (x', y', s', W') that satisfies all integrality and feasibility constraints.

Step 1: Adaptive Station Selection for Household Coverage

At the outset, we start with a candidate set of open stations $\{j \in \mathcal{J} \mid y_j^t = 1\}$ derived from the Lagrangian solutions. This set may initially be empty (if no station was selected by the subproblem solutions), partially cover the households (if some are covered and some are not), or already fully cover all households. Our adaptive station selection heuristic ([Algorithm 2](#)) is designed to handle all three scenarios while respecting the natural constraint that no more than $|\mathcal{J}|$ stations can be opened in total.

At any given iteration, let $\mathcal{U}^c \subseteq \mathcal{I}$ denote the set of uncovered households. For each unopened station $j \in \mathcal{J}$, we compute a weight $w_j = |\mathcal{I}_j \cap \mathcal{U}^c|$, representing how many uncovered households could be covered by station j . Stations that cannot cover any uncovered households are ignored. Among the candidate stations, the algorithm selects one to open based on probabilities proportional to the weights w_j . This probabilistic selection approach reduces the risk of biases and prevents repeatedly opening the same or suboptimal stations.

By construction, [Algorithm 2](#) must terminate with $\mathcal{U}^c = \emptyset$. Specifically, if at some point no candidate stations remained to cover \mathcal{U}^c , it would imply that each uncovered household had no accessible station in its predefined neighborhood \mathcal{J}_i . However, [Algorithm 1](#) ensures $\mathcal{J}_i \neq \emptyset$ for every household i , making such a scenario impossible. Therefore, with each station opening strictly reducing $|\mathcal{U}^c|$ by at least one, and given that we cannot open more than $|\mathcal{J}|$ stations, we must achieve full coverage of all households within at most $|\mathcal{I}|$ iterations. Hence, the algorithm ends with $\mathcal{U}^c = \emptyset$, ensuring that every household is covered by at least some open station. While this coverage alone does not guarantee feasible assignments under all constraints (e.g., charger capacities and waiting times), it establishes a fully covered station configuration for subsequent assignments.

Step 2: Household Assignment to Stations and Chargers

In Step 2 our goal is to transform the fractional assignment results x_{ijk}^t from the subproblem solutions SP_j into integral assignments $x'_{ijk} \in \{0, 1\}$ that satisfy all the constraints. [Algorithm 3](#) manages this task. We prioritize households by sorting them in descending order of their demand rates λ_i , thus addressing the most demanding households first. For each household i , we consider those stations j that are open ($y'_j = 1$) and accessible to i ($j \in \mathcal{J}_i$). We then generate a candidate list \mathcal{C}_i of all station-charger pairs (j, k) that are both open and capable of serving household i . To select a suitable (j, k) from \mathcal{C}_i , we impose a heuristic sorting that considers the following:

1. The fractional assignments x_{ijk}^t from the subproblem solutions, leveraging prior knowledge about the likelihood of a successful integral assignment
2. Charger usage counts n_{jk} and installation costs C_k^ξ , guiding us toward cost-effective and less congested chargers
3. Current waiting times W_{jk} , ensuring that we assign households to station-charger pairs that can meet the waiting time constraints

This ordered candidate list is processed by the CHECKANDASSIGN subroutine ([Algorithm 4](#)), which attempts to fix $x'_{ijk} = 1$ while adjusting the number of chargers s'_{jk} and updating W'_{jk} to maintain feasibility. If an appropriate (j, k) is found, household i is successfully assigned. Otherwise, if no candidate pair meets all constraints, the household is added to the set \mathcal{U}^a of unassigned households for further handling in subsequent steps.

Step 3: Adjusting for Overload and Ensuring Final Feasibility

If after attempting the assignment, some households remain unassigned ($\mathcal{U}^a \neq \emptyset$), we attempt to open additional stations to reduce overload and accommodate these households. [Algorithm 5](#) chooses additional stations, if possible, to support the uncovered demand. After updating the station configuration, we rerun the household assignment iteration until no further improvements are possible. This iterative refinement ensures that we eventually reach a stable configuration where all households are assigned.

Once every household i is assigned, we verify that the number of chargers s'_{jk} and expected waiting times W'_{jk} are consistent with the constraints. The computations for s'_{jk} and W'_{jk} follow directly from the final assignments and the queuing system constraints integrated into CHECKANDASSIGN. We produce a feasible solution $(x'_{ijk}, y'_j, s'_{jk}, W'_{jk})$ for \mathbb{G} .

5.6 Combining Cutting-Planes Approach, Subgradient Method, and Rounding Heuristic

At any iteration t , given Lagrangian multipliers $\eta^t = (\zeta^t, \theta^t, \beta_\phi^t, \beta_\xi^t, \nu^t)$, we solve all subproblems SP_j for each $j \in \mathcal{J}$ in parallel in Step 2. This produces solutions $(x_{ijk}^t, y_j^t, s_{jk}^t, W_{jk}^t)$ and a Lagrangian value $\mathcal{L}(\eta^t)$, providing a lower bound on \mathbb{G} . We then apply a rounding heuristic to these fractional solutions, yielding an integral feasible solution with objective value UB^t . The primal-dual gap at iteration t is $\Delta^t = 1 - \frac{\mathcal{L}(\eta^t)}{UB^t}$. If $\Delta^t > \delta$, where $\delta > 0$ is a specified convergence criterion, we update the Lagrangian multipliers η^t using the subgradient method and, if necessary, refine the upper bound UB^t . We then re-solve the subproblems SP_j in parallel with these updated multipliers for potentially reducing the gap. This iterative process continues until $\Delta^t \leq \delta$. In practice, convergence may be determined either by reaching the specified tolerance δ or by imposing

computational limits, such as a maximum number of iterations or a time budget. By adapting the multipliers at each iteration and repeatedly solving the subproblems with refined multipliers, we ensure that our method eventually produces a high-quality solution, making it suitable for extreme-scale SCLA instances. We provide additional details about our parallel computing implementation in Section 6.4.

6 Computational Experiments

All experiments were conducted on Intel Xeon CPU 6248R. We use Gurobi 10.0.2 (Gurobi Optimization, LLC 2024) as the MIQP and MIP solver, and we use mpi4py (Dalcín et al. 2008) for parallel processing.

6.1 Design of Experiments

To test our proposed frameworks’ ability to solve extreme-scale SCLA problem instances, we conduct computational experiments using data from the Chicago metropolitan area. We utilize e-commerce daily demand information and road network data, both sourced from POLARIS (Planning and Operations Language for Agent-based Regional Integrated Simulation). POLARIS is an advanced simulation tool developed by researchers at Argonne National Laboratory (Auld et al. 2016).

We defined six scenarios based on two key factors: charging locations and policy frameworks. For charging locations, planners can install chargers at traffic analysis zone (TAZ) sites, existing depots, or a combination of both. Regarding policy frameworks, scenarios use either single-agency or multiagency operations. Under single-agency operation, each household belongs to exactly one agency and may use only that agency’s stations (depot or TAZ). Under multiagency collaboration, however, all depots are pooled across agencies, and TAZ-based stations carry no agency affiliation; thus every household can access any open station, whether it is at a depot or a TAZ.

Figure 1 shows the spatial distribution of households and candidate charging stations across the Chicago metropolitan area. The map Figure 1 (a) highlights potential charging stations (squares) located at centroids of TAZs. Existing depots for four major agencies—Amazon, FedEx, UPS, and USPS—are depicted with larger symbols of distinct shapes and colors (e.g., black circles for Amazon, orange hexagons for FedEx). These depots can also be used as candidate station sites, although their station-opening cost C^ϕ is zero.

The map Figure 1 (b) overlays the same TAZ grid but now includes the potential station locations via depots and TAZs, again color-coded by agency affiliation. Each agency represents a single subscription policy in one scenario (restricting households to use that agency’s stations) or participates in a multiagency collaboration in other scenarios. The dataset consists of 449,367 households, 1,958 potential station sites (TAZ centroids), and 53 existing depots, making it the largest known instance for a queue-based charger location-allocation study.

The problem parameters used are based on the literature (Rivian EDV 2024, Upper Inc. 2024, Davatgari 2021, Electrify America 2024, Lightning eMotors 2022, Smith and Castellano 2015, Williams 2020). To compute the detour and waiting costs per minute, we utilized financial and operational data from FedEx (FedEx 2024a,b,c,d) and UPS (Upper Inc. 2024). The detour cost was derived by looking at FedEx’s revenue metrics. We calculate the revenue per vehicle per day by distributing FedEx’s annual revenue over its operating days and fleet size, assuming that any detour could potentially cut into this daily revenue, thereby translating into a cost. For the waiting cost, we based our calculation on the hourly wage rate of UPS drivers, treating time spent waiting as a direct labor cost. By estimating the cost per minute from the hourly wage, we capture the

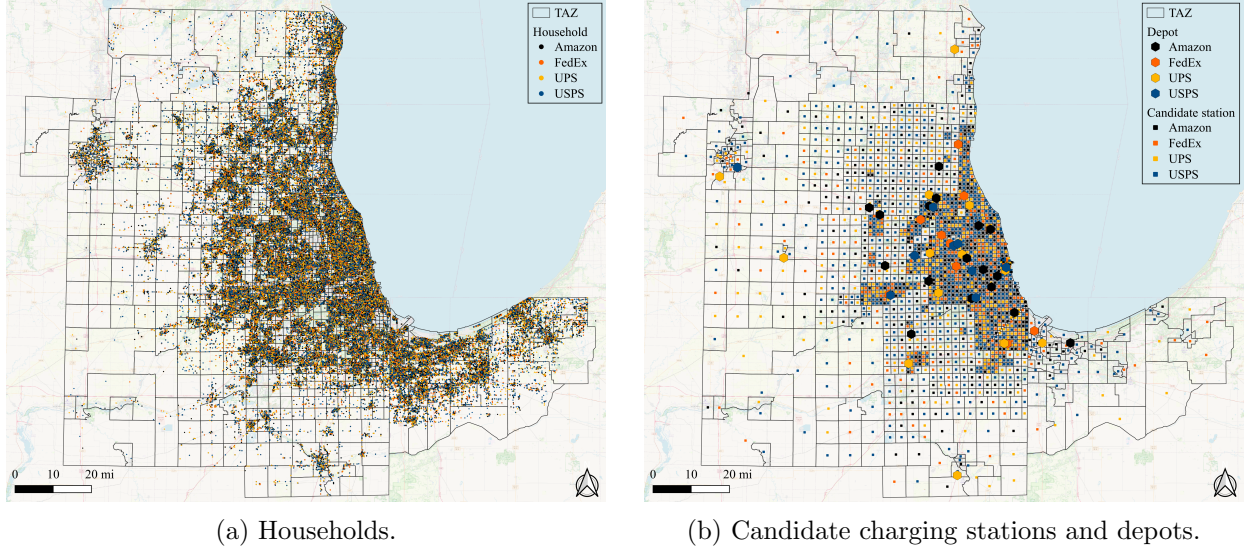


Figure 1: Illustration of the spatial distribution of households, potential charging stations, and existing charging depots across the Chicago metropolitan area.

Table 2: General parametric values

C^ϕ (USD)	C^δ (USD/min)	C^τ (USD/min)	B^ϕ (USD/day)	B^ξ (USD/day)	\bar{Y} (units)	EW (min)	Lifetime (years)
1,000,000	1.09	0.70	150,000	500,000	1000	30	40

expenses incurred during periods when drivers are idle. Alongside these costs, μ_k quantifies the number of full charging cycles that each type of charger can complete in one minute. It is calculated by dividing the total charging capacity needed to fully charge a vehicle from a specific initial SOC by the charger’s power output. The result is then converted from the total time required to charge (in seconds) to how many cycles can be completed per minute; the parameters are summarized in [Table 2](#).

For simplicity, we assume each vehicle completes exactly one charging stop per day, making $1/\nu$ the fraction of deliveries that need a charge, where ν is the average number of deliveries per vehicle per day derived from historical data. Hence, for household i , $N_i^C = N_i^D/\nu$, leading to $\pi_i = N_i^C/N_i^D = 1/\nu$. Finally, $\lambda_i = \gamma_i \pi_i$ is the overall charging rate for that household.

Our analysis incorporates three charger types of varying power outputs along the same lines in the literature ([Liu and Wang 2017](#), [Yilmaz and Krein 2012](#)). In order to standardize the objective function, all costs are converted to USD per day. This conversion assumes lifespans of 10 years for chargers and 40 years for facilities, based on estimates by [Bennett et al. \(2022\)](#). [Table 3](#) presents a summary of the charger-specific parameters.

Table 3: Charger-specific parametric values

Type	C^ξ (USD)	Power (kWh)	μ_k (charging/min)	\bar{S}_{jk} (units)	Lifetime (years)
Basic	73,000	50	0.53	20	10
Moderate	157,000	180	1.90	20	10
Fast	228,000	360	3.81	20	10

6.2 Computational Performance of Exact Cutting-Planes Method and Lagrangian Dual Decomposition Approach

To effectively solve the SCLA problem, we first develop an understanding of our solution methods by analyzing the computational performance of our exact cutting planes approach and comparing it with the Lagrangian dual decomposition method. This analysis utilizes cardinality of \mathcal{J} , k_c , and \mathcal{I} as key determinants of problem size. A testbed of instances was generated by utilizing e-commerce daily demand information and road network data of the Chicago metropolitan area serving e-commerce deliveries from POLARIS (Auld et al. (2016)). As a baseline, the parametric design provided in Section 6.1 was utilized.

For the computational study in this section we focus on the central section of Cook County around the Chicago Loop area, which includes $|\mathcal{J}| = 20$ potential charging locations. We assume a multiagency policy, meaning any open station whether at a TAZ or an existing depot can serve any household. Within this region, we sample $|\mathcal{I}|$ households. Details of each scenario appear in Table 4.

We compare four different approaches to solve five instances of a specific scenario with a time limit of 1 hour. The first method, denoted as E_{MIQP} , directly solves the exact MIQP formulation. It provides valid upper and lower bounds denoted $\text{UB}^{E_{\text{MIQP}}}$ and $\text{LB}^{E_{\text{MIQP}}}$, respectively. The second method, denoted as E_{MCC} , relaxes the MIQP objective by replacing bilinear $W_{jk}x_{ijk}$ terms with McCormick envelopes. This approach yields a valid lower bound $\text{LB}^{E_{\text{MCC}}}$ but requires recalculating the true upper bound $\text{UB}^{E_{\text{MCC}}}$ with respect to the original MIQP objective (equation 3). The third method, denoted as L_{BIL} , employs Lagrangian dual decomposition where the subproblems SP_j are solved by using the bilinear formulation. It produces a valid lower bound $\text{LB}^{L_{\text{BIL}}}$ from the Lagrangian dual problem and obtains a valid upper bound $\text{UB}^{L_{\text{BIL}}}$ via primal heuristics. The fourth method, denoted as L_{MCC} , is similar to L_{BIL} but solves the subproblems SP_j by relaxing the bilinear term $W_{jk}x_{ijk}$ with McCormick envelopes. This method provides a lower bound $\text{LB}^{L_{\text{MCC}}}$ and an upper bound $\text{UB}^{L_{\text{MCC}}}$ again via primal heuristic. For each method we calculate the model gap, denoted as Gap^m , where $m \in \{E_{\text{MIQP}}, E_{\text{MCC}}, L_{\text{BIL}}, L_{\text{MCC}}\}$. The model gap is calculated as $\text{Gap}^m = \frac{|\text{UB}^m - \text{LB}^m|}{\text{UB}^m} \times 100\%$. For the first method, E_{MIQP} , the model gap $\text{Gap}^{E_{\text{MIQP}}}$ is straightforward to compute since both the upper and lower bounds $\text{UB}^{E_{\text{MIQP}}}$ and $\text{LB}^{E_{\text{MIQP}}}$ are directly obtained from the solver. In the second method E_{MCC} , the upper bound $\text{UB}^{E_{\text{MCC}}}$ is recalculated with the original MIQP objective (Equation 3) to accurately calculate $\text{Gap}^{E_{\text{MCC}}}$. For both Lagrangian methods L_{BIL} and L_{MCC} the valid upper and lower bounds UB^m and LB^m allow for direct calculation of the primal dual gaps $\text{Gap}^{L_{\text{BIL}}}$ and $\text{Gap}^{L_{\text{MCC}}}$. By comparing the model gaps across these four methods, we can analyze their computational performance and effectiveness in solving five instances of SCLA of a particular scenario. Additionally we introduce a secondary gap metric Gap_m^t to assess each method against the tightest lower bound achieved across all approaches. This bound LB^* is the maximum of all lower bounds: $LB^* = \max\{\text{LB}^{E_{\text{MIQP}}}, \text{LB}^{E_{\text{MCC}}}, \text{LB}^{L_{\text{BIL}}}, \text{LB}^{L_{\text{MCC}}}\}$. Using LB^* , we calculate Gap_m^t by comparing each method's upper bound and calculate $\text{Gap}_m^t = \frac{|\text{UB}^m - LB^*|}{\text{UB}^m} \times 100\%$. This metric provides a measure of how each method's upper bound approaches the best-known lower bounds. By making use of both Gap^m and Gap_m^t , we gain an understanding of the computational performance and efficiency of each method in solving the SCLA problem. We average the Gap^m and Gap_m^t over five instances of a particular scenario and report the results in Table 4.

In Table 5 we compare the problem sizes in terms of integer, binary, and continuous variables for all four methods E_{MIQP} , E_{MCC} , L_{BIL} , and L_{MCC} across various scenarios characterized by $|\mathcal{I}|$ and k_c . To assess the worst-case computational burden within the Lagrangian framework, we identify SP_j^{max} as the subproblem with the largest number of continuous variables among all subproblems SP_j for each scenario. We detail this comparison in Table 5. In Table 6 we present the number of

Table 4: Comparison of MIQP and Lagrangian solution methods

Scenario		E _{MIQP}		E _{MCC}		L _{BIL}		L _{MCC}	
$ \mathcal{I} $	k_c	Gap ^m (%)	Gap ^t (%)	Gap ^m (%)	Gap ^t (%)	Gap ^m (%)	Gap ^t (%)	Gap ^m (%)	Gap ^t (%)
50	1	<1	<1	<1	<1	<1	<1	<1	<1
100	1	<1	<1	<1	<1	<1	<1	4.08	<1
200	1	17.67	<1	3.91	<1	<1	<1	12.49	<1
400	1	37.80	<1	24.75	<1	<1	<1	27.69	<1
800	1	55.94	1.03	53.44	<1	<1	<1	46.79	<1
1600	1	74.84	1.12	68.28	<1	<1	<1	65.47	<1
3200	1	85.80	<1	82.27	1.26	<1	<1	79.82	<1
50	2	<1	<1	<1	<1	1.73	1.42	6.19	<1
100	2	3.79	<1	1.36	<1	5.38	5.06	10.20	<1
200	2	18.81	1.21	16.71	1.24	14.26	14.26	18.59	1.23
400	2	41.44	1.51	39.00	4.54	16.46	16.46	34.11	1.59
800	2	62.49	2.25	55.53	3.5	20.49	20.49	52.39	3.06
1600	2	73.28	2.17	71.19	2.45	30.22	30.22	69.38	2.46
3200	2	85.60	25.86	88.21	40.66	50.12	50.12	82.62	21.84
50	4	<1	<1	<1	<1	5.35	4.25	10.00	1.75
100	4	9.40	<1	6.65	<1	4.37	4.24	17.33	<1
200	4	31.93	1.41	31.19	1.49	8.17	8.17	34.53	3.13
400	4	58.88	13.08	49.26	3.41	10.59	10.59	49.40	4.94
800	4	66.93	3.66	63.84	4.65	14.96	14.96	68.14	10.41
1600	4	81.12	7.72	78.21	9.23	26.91	26.91	80.13	9.80
3200	4	90.73	33.12	91.08	38.65	57.31	57.31	89.96	23.94
50	8	1.24	<1	<1	<1	7.11	6.12	18.60	4.61
100	8	22.70	3.69	20.77	3.83	14.68	14.68	30.71	6.30
200	8	44.25	8.68	37.87	8.78	22.56	22.56	48.60	16.03
400	8	58.22	8.16	52.06	8.60	24.36	24.36	61.89	16.69
800	8	74.92	7.30	68.79	7.32	29.25	29.25	73.66	15.69
1600	8	85.39	23.14	83.23	26.39	61.19	61.19	85.30	27.81
3200	8	93.10	48.01	92.89	51.43	86.47	86.70	92.77	46.47

instances (out of five) where each method achieved the tightest upper bound (within 1%) within one hour. In the subsequent subsections, we discuss insights from the computational experiments detailed in [Section 6.2](#).

6.2.1 Effect of k_c and $|\mathcal{I}|$ on Model Gap (Gap^m)

For the exact methods (E_{MIQP} and E_{MCC}), the model gap Gap^m remains low (less than 1%) for small problem sizes (e.g., $|\mathcal{I}| = 50$ and $k_c = 1$). As $|\mathcal{I}|$ increases, however, Gap^m increases significantly. For instance, at $|\mathcal{I}| = 200$ and $k_c = 1$, E_{MIQP} has a Gap^m of 17.67%, while E_{MCC} improves on this with a gap of 3.91%. When $|\mathcal{I}| = 3200$, the gaps become substantial, exceeding 80% for both exact methods, indicating that they struggle to find tight lower bounds within the time limit for larger problems. Increasing k_c exacerbates the computational difficulty for the exact methods. With more charging stations considered per household, the problem’s connectivity increases, leading to a higher number of variables and constraints (see [Table 5](#)). For example, at $|\mathcal{I}| = 200$ and $k_c = 8$,

Table 5: Problem size comparison of MIQP and Lagrangian relaxation methods

Scenario		E _{MIQP}		E _{MCC}		Master (Cont.)	L _{BIL} SP_j^{max}		L _{MCC} SP_j^{max}	
$ \mathcal{I} $	k_c	Int. (Bi)	Cont.	Int. (Bi)	Cont.		Int. (Bi)	Cont.	Int. (Bi)	Cont.
50	1	1490 (1430)	60	1490 (1430)	210	54	67 (64)	39	67 (64)	75
100	1	1640 (1580)	60	1640 (1580)	360	104	67 (64)	69	67 (64)	135
200	1	1940 (1880)	60	1940 (1880)	660	204	67 (64)	120	67 (64)	237
400	1	2540 (2480)	60	2540 (2480)	1260	404	67 (64)	243	67 (64)	483
800	1	3740 (3680)	60	3740 (3680)	2460	804	67 (64)	477	67 (64)	951
1600	1	6140 (6080)	60	6140 (6080)	4860	1604	67 (64)	891	67 (64)	1779
3200	1	10940 (10880)	60	10940 (10880)	9660	3204	67 (64)	1707	67 (64)	3411
50	2	1556 (1496)	60	1556 (1496)	276	54	67 (64)	45	67 (64)	87
100	2	1808 (1748)	60	1808 (1748)	528	104	67 (64)	72	67 (64)	141
200	2	2249 (2189)	60	2249 (2189)	969	204	67 (64)	150	67 (64)	297
400	2	3197 (3137)	60	3197 (3137)	1917	404	67 (64)	294	67 (64)	585
800	2	5081 (5021)	60	5081 (5021)	3801	804	67 (64)	615	67 (64)	1227
1600	2	8807 (8747)	60	8807 (8747)	7527	1604	67 (64)	1197	67 (64)	2391
3200	2	16226 (16166)	60	16226 (16166)	14946	3204	67 (64)	2325	67 (64)	4647
50	4	1757 (1697)	60	1757 (1697)	477	54	67 (64)	69	67 (64)	135
100	4	2204 (2144)	60	2204 (2144)	924	104	67 (64)	129	67 (64)	255
200	4	3068 (3008)	60	3068 (3008)	1788	204	67 (64)	234	67 (64)	465
400	4	4736 (4676)	60	4736 (4676)	3456	404	67 (64)	420	67 (64)	837
800	4	8090 (8030)	60	8090 (8030)	6810	804	67 (64)	822	67 (64)	1641
1600	4	14918 (14858)	60	14918 (14858)	13638	1604	67 (64)	1665	67 (64)	3327
3200	4	28517 (28457)	60	28517 (28457)	27237	3204	67 (64)	3327	67 (64)	6651
50	8	2033 (1973)	60	2033 (1973)	753	54	67 (64)	87	67 (64)	171
100	8	2747 (2687)	60	2747 (2687)	753	104	67 (64)	171	67 (64)	339
200	8	4049 (3989)	60	4049 (3989)	2769	204	67 (64)	336	67 (64)	669
400	8	6704 (6644)	60	6704 (6644)	5424	404	67 (64)	648	67 (64)	1293
800	8	12263 (12203)	60	12263 (12203)	10983	804	67 (64)	1308	67 (64)	2613
1600	8	23207 (23147)	60	23207 (23147)	21927	1604	67 (64)	2496	67 (64)	4989
3200	8	44453 (44393)	60	44453 (44393)	43173	3204	67 (64)	4896	67 (64)	9789

E_{MIQP} exhibits a Gap^m of 44.25%, and E_{MCC} has a gap of 37.87%. At $|\mathcal{I}| = 3200$ and $k_c = 8$, the model gaps reach over 92% for both methods. The Lagrangian methods (L_{BIL} and L_{MCC}) display better scalability with respect to $|\mathcal{I}|$ and k_c . L_{BIL} maintains low model gaps for small k_c values across all $|\mathcal{I}|$. Even at $|\mathcal{I}| = 3200$ and $k_c = 1$, L_{BIL} achieves a Gap^m of less than 1%. As k_c increases, however, the model gaps for Lagrangian methods also increase but remain lower than those of the exact methods. For high k_c values, L_{MCC} sometimes outperforms L_{BIL} in reaching tighter upper bounds.

6.2.2 Gap Relative to Tightest Lower Bound (Gap^t)

For the exact methods (E_{MIQP} and E_{MCC}), Gap^t is generally significantly lower than their model gaps Gap^m, especially in larger problem instances. The reason is that while the exact methods may struggle to find tight lower bounds themselves, they benefit from the tighter lower bounds obtained by the Lagrangian methods, particularly L_{MCC}. Examining Table 4, at $|\mathcal{I}| = 200$ and $k_c = 1$, we see that E_{MIQP} has a model gap Gap^m of 17.67%, but its gap relative to the tightest lower bound Gap^t is less than 1%. This significant reduction indicates that another method (L_{BIL}

Table 6: Number of instances each method reached the tightest upper bound within 1 hour

$ \mathcal{I} $	k_c	EMIQP	EMCC	LBIL	LMCC
50	1	5/5	5/5	5/5	5/5
100	1	5/5	5/5	5/5	5/5
200	1	4/5	5/5	5/5	5/5
400	1	5/5	3/5	5/5	5/5
800	1	3/5	5/5	5/5	5/5
1600	1	3/5	5/5	5/5	5/5
3200	1	4/5	3/5	5/5	5/5
50	2	5/5	5/5	3/5	4/5
100	2	5/5	5/5	1/5	5/5
200	2	5/5	5/5	0/5	5/5
400	2	5/5	4/5	0/5	5/5
800	2	5/5	4/5	0/5	2/5
1600	2	5/5	4/5	0/5	4/5
3200	2	0/5	0/5	0/5	5/5
50	4	5/5	5/5	3/5	4/5
100	4	5/5	5/5	3/5	4/5
200	4	5/5	5/5	0/5	2/5
400	4	4/5	5/5	1/5	2/5
800	4	4/5	4/5	0/5	0/5
1600	4	3/5	4/5	0/5	0/5
3200	4	0/5	0/5	0/5	5/5
50	8	5/5	5/5	3/5	3/5
100	8	5/5	5/5	0/5	2/5
200	8	5/5	4/5	1/5	1/5
400	8	5/5	4/5	0/5	0/5
800	8	5/5	5/5	0/5	0/5
1600	8	3/5	3/5	0/5	0/5
3200	8	1/5	1/5	0/5	4/5
Total		114/140	113/140	50/140	93/140

in this case) has provided a much tighter lower bound, effectively improving the perceived quality of E_{MIQP} 's solution when compared with the best-known solution. As the problem size increases, the contribution of the Lagrangian methods to the tightest lower bound becomes greater. Specifically, L_{MCC} demonstrates better performance in providing tight lower bounds for larger problem instances with higher k_c values. For example, at $|\mathcal{I}| = 3200$ and $k_c = 8$, L_{MCC} achieves a Gap^m of 92.77% and a Gap^t of 46.47%, which is significantly better than the exact methods. In contrast, E_{MIQP} has a Gap^m of 93.10% and a Gap^t of 48.01%, indicating that L_{MCC} has provided a tighter lower bound that benefits all methods when computing Gap^t . Furthermore, Table 6 shows that L_{MCC} reaches the tightest upper bound in 4 out of 5 instances at $|\mathcal{I}| = 3200$ and $k_c = 8$, outperforming the exact methods, which achieve this only in 1 out of 5 instances. This demonstrates L_{MCC} 's effectiveness not only in providing tight lower bounds but also in finding high-quality feasible solutions in large problems.

6.2.3 Problem Size Comparison

From [Table 5](#) we can see that for the exact methods (E_{MIQP} and E_{MCC}), the number of integer variables escalates dramatically as both the number of households $|\mathcal{I}|$ and the number of nearest charging stations k_c increase. For instance, at $|\mathcal{I}| = 3200$ and $k_c = 8$, the exact methods require over 44,000 integer variables and approximately 43,000 continuous variables. Constructing such large MIQP models is not only computationally intensive but often infeasible in practice because of memory limitations and processing constraints of optimization solvers such as Gurobi. In many cases, especially at this scale, the solver cannot even build the full model, rendering the exact methods impractical for large-scale problems. In contrast, the Lagrangian methods (L_{BIL} and L_{MCC}) decompose the original problem into smaller, more manageable subproblems SP_j , each associated with a charging station $j \in \mathcal{J}$. The master problem remains relatively small, containing only continuous variables (e.g., 3,204 variables when $|\mathcal{I}| = 3200$). Each subproblem SP_j involves a fixed number of integer variables (67 in all scenarios) and a manageable number of continuous variables that scale linearly with $|\mathcal{I}|$ and k_c . However, since the number of households associated with each charging station varies, the size of each subproblem SP_j can differ. Specifically, at $|\mathcal{I}| = 3200$ and $k_c = 8$, the largest subproblem SP_j^{max} in L_{MCC} has only 67 integer variables and approximately 9,789 continuous variables. In [Table 5](#) we report the problem size for SP_j^{max} to illustrate the maximum computational effort required for any single subproblem within each scenario. This decomposition significantly reduces the computational burden, enabling the Lagrangian methods to handle extremely large-scale instances effectively where the exact methods cannot even construct the model. The sharp contrast in problem sizes highlights the scalability advantage of the Lagrangian methods. While the exact methods' problem size grows exponentially with $|\mathcal{I}|$ and k_c , making them unsuitable for large problems, the Lagrangian methods maintain a linear growth in subproblem sizes. By focusing on the maximum subproblem size SP_j^{max} , we demonstrate that even the most demanding subproblem remains computationally tractable. Thus, the Lagrangian methods to exploit problem structure and computational resources more efficiently, being able to solve instances that are beyond the capability of the exact methods.

6.2.4 Ability to Reach the Tightest Upper Bound

From [Table 6](#), we can see that the exact methods achieve the tightest upper bound consistently in smaller problem instances. However, their performance deteriorates as both $|\mathcal{I}|$ and k_c increase. For example, at $|\mathcal{I}| = 3200$ and $k_c = 8$, E_{MIQP} reaches the tightest upper bound in only one out of five instances. In contrast, the Lagrangian methods demonstrate superior performance in larger instances. Specifically, L_{MCC} reaches the tightest upper bound in four out of five instances at $|\mathcal{I}| = 3200$ and $k_c = 8$, outperforming all other methods. This result shows the effectiveness of the Lagrangian dual decomposition approach in scenarios that are both large scale and highly connected. While the exact methods are well suited for small-scale problems with a low k_c , providing high-quality solutions within reasonable computational times, they suffer from a lack of scalability due to the exponential increase in problem size with larger $|\mathcal{I}|$ and k_c . On the other hand, the Lagrangian methods, which leverage problem decomposition, offer a scalable alternative capable of handling larger problem instances effectively. They maintain acceptable model gaps and are likely to reach an acceptable upper bound within the given time limit, especially in scenarios with a high k_c . The choice between bilinear subproblems and McCormick relaxation within the Lagrangian framework depends on the specific scenario, where L_{BIL} tends to perform better for small to moderate k_c values, while L_{MCC} may be more advantageous for higher k_c values in terms of reaching the tightest upper bounds.

6.3 Charging Location Strategies and Policy Frameworks

In this section we analyze the impact of different charging location strategies and policy frameworks on the objective (3). By evaluating various scenarios, we aim to provide managerial insights into optimizing infrastructure investments and operational policies. The combination of charging location strategies and management policies enables us to evaluate their combined impact on the total objective of SCLA (objective 3).

Table 7: Percentage change in the objective for various scenarios using L_{MCC} method

Scenario	Charging Location		Policy		% \uparrow in \mathbb{C}			
	TAZs	Depots	Single	Multi	Mean	Std Dev	Min	Max
1	✓	×	✓	×	91.24	7.82	82.79	100.74
2	✓	×	×	✓	44.82	10.08	32.61	62.46
3	×	✓	✓	×	42.33	11.14	27.39	60.93
4	×	✓	×	✓	32.23	3.95	25.34	35.93
5	✓	✓	✓	×	14.51	3.97	8.07	19.18
6	✓	✓	×	✓	-	-	-	-

Table 7 demonstrates that strategic decisions on charging infrastructure placement at new locations (TAZs) versus existing facilities (depots) and operational policies significantly impact total costs compared with the baseline configuration (Scenario 6). For each scenario we generate five random instances with 100 households each ($|\mathcal{I}| = 100$), and the results presented are averaged over these five instances. To account for detour times across all households, we scale the detour cost parameter C^δ by a fixed multiplier. The transition from Scenario 6 (optimal baseline) to Scenario 5 involves switching from multiagency to single-agency policy while keeping combined TAZs and depot locations, which increases total costs by 14.51%. The switch from the baseline to Scenario 4 restricts charging stations to only existing depot locations under a multiagency policy and increases costs by 32.23%. Scenario 3 applies a single-agency policy to depot-only locations, which increases costs by 42.33%. Similarly, Scenario 2 constrains locations to only new potential TAZ locations while maintaining a multiagency policy, which drives costs up by 44.82%. Scenario 1 represents the most restrictive case, combining TAZ-only locations with single-agency policy, which produces the highest cost increase of 91.24% from the baseline.

This systematic pattern of cost increases across scenarios offers key insights for infrastructure planning and policy development. The cost increase from the baseline Scenario 6 to Scenario 1 (91.24%) demonstrates how limiting charging infrastructure to only new locations and restricting operational flexibility through single-agency policy lead to substantial cost increases. Policymakers should recognize that the shift from multiagency policy alone (Scenario 5) produces the smallest cost increase, whereas restricting charging stations to either only new locations or only existing facilities creates larger cost impacts. We believe that for long-term sustainability policymakers should prioritize implementation plans that consider both new potential locations (TAZs) and existing facilities (depots) for charging infrastructure development rather than restricting installations to only existing facilities. Our analysis demonstrates that combining charging station placement at new strategic locations with existing depot facilities while enabling multiagency collaborative operations leads to the most cost-effective outcomes.

6.4 Large-Scale Case Study

Building on the insights from the preceding section, which demonstrated the scalability and effectiveness of Lagrangian methods combined with primal heuristics in solving large-scale SCLA problems, we present a comprehensive large-scale case study. The dataset includes 449,367 households, 1,958 potential charging stations, and 53 existing charging depots. This dataset represents the largest ever used in studies of charger location allocation with queue congestion. We assume a multiagency policy, meaning any open station whether at a TAZ or an existing depot can serve any household. To tackle this extensive problem, we apply the Lagrangian dual decomposition approach, employing the McCormick relaxation subproblem formulation (L_{MCC}).

6.4.1 Multipartition Parallelization Strategy

In our large-scale SCLA implementation, we faced the challenge of solving 2011 station-level subproblems $\{SP_j : j \in \mathcal{J}\}$ across a heterogeneous HPC environment. While an ideal solution would allocate one CPU core per subproblem for simultaneous execution, our available HPC infrastructure consisted of three distinct partitions with more limited resources. The Short Partition (P_S) provided 400 CPU cores with a one-hour runtime limit, while the Group Partition (P_G) provided 180 CPU cores without time constraints, and the Open Partition (P_O) provided 100 CPU cores with a 48-hour time limit. Communication between these partitions is not possible in our HPC environment. This resource configuration requires strategic distribution of the subproblems across partitions. An example allocation may look like assigning approximately 800 subproblems to P_G , 600 to P_O , and the remaining 611 to P_S . The exact numbers may vary, but each partition faces more subproblems than CPU cores; and so, to address this situation, we employ a hierarchical master-worker architecture and a partitioning and scheduling strategy.

Global master (Lagrangian dual controller) : The *global master* runs on one of the cores in the group partition P_G . It initializes the multipliers $(\zeta, \theta, \beta_\phi, \beta_\xi, \nu)$ and randomly partitions \mathcal{J} into three subsets $\mathcal{J}_S, \mathcal{J}_G, \mathcal{J}_O$, assigning each subset to P_S, P_G , and P_O , respectively. Each subproblem SP_j is defined over a station j , its corresponding set \mathcal{I}_j of households, and multiple charger types, resulting in varying problem sizes and complexities across the subproblems.

Partition masters and workload distribution : Within each partition, a *partition master* receives its assigned subset of subproblems \mathcal{J}_p ($p \in \{S, G, O\}$). Since $|\mathcal{J}_p|$ exceeds the available CPU cores in each partition, the partition master must distribute multiple subproblems to each worker. For load balancing, we first sort the subproblems in \mathcal{J}_p by descending order of $|\mathcal{I}_j|$ (number of households assigned to location j), using this as a proxy for computational complexity. The sorted subproblems are then distributed once using round-robin assignment: if there are w workers, worker i receives its complete batch of problems $\{j_i, j_{i+w}, j_{i+2w}, \dots\}$.

Execution and completion of subproblems : Each worker then processes its assigned batch independently, without further communication with the *partition master*. The *partition master* simply waits for all workers to complete their assigned problems before declaring completion. If any subproblem assigned P_S fails to complete, its index is recorded, and the *global master* subsequently resubmits it to the group partition P_G . This mechanism ensures that every subproblem is ultimately solved.

Iterative updates by the global master : After all subproblems in $\mathcal{J}_S, \mathcal{J}_G, \mathcal{J}_O$ are completed, the global master collects the results. At this stage, it performs subgradient updates, considering a subgradient calculation time T^{subgrad} , and executes primal heuristics with a heuristic execution time $T^{\text{heuristic}}$. These adjustments to the multipliers may prompt another iteration of subproblem assignments or lead to termination once convergence criteria are met. Our multipartition parallelization strategy leverages random partitioning of \mathcal{J} , hierarchical control, sorted-round-robin scheduling, and a mechanism for reassigning failed tasks. Even with far fewer cores than subproblems and differing time limits and complexities, this approach allows us to efficiently and systematically solve all subproblems over time. This enables the *global master* to advance through the Lagrangian dual iterations. We present the results below.

Table 8: Large-scale case study results using the L_{MCC} method with a 6-hour time limit

Charging Location		Policy		$ \mathcal{J} $	J^{open}	Total Chargers ($\sum_{j \in \mathcal{J}} S_{jk}$)			\bar{W}_{jk} (min)			Gap ^m (%)
TAZs	Depots	Single	Multi			k_1	k_2	k_3	k_1	k_2	k_3	
✓	✓	×	✓	2014	436	218	109	302	123.57	31.53	16.59	78.5

k_1 : Slow chargers, k_2 : Moderate chargers, k_3 : Fast chargers.

From Table 8 we observe the results of our large-scale SCLA implementation, which successfully solved an instance with 449,367 households and 2,014 potential station locations (including both TAZs and existing depots). Using a 6-hour time limit and the McCormick relaxation (L_{MCC}) formulation, the method identified 436 best station locations out of 2,014 candidates, requiring only 21.6% of the available sites. Across these opened stations, a total of 629 chargers were deployed—218 slow chargers, 109 moderate chargers, and 302 fast chargers—indicating a preference for higher-speed charging options in the best configuration.

Slow chargers averaged 1.36 chargers per station, with a combined waiting and service time (system time) of 123.58 minutes. Moderate chargers averaged 1.00 charger per station and achieved a shorter system time of 31.53 minutes. Fast chargers also averaged 1.00 charger per station, providing the lowest system time of just 16.60 minutes. From a computational perspective, the maximum Gurobi solve time per subproblem was 3019.04 seconds, and the primal heuristic phase was completed in 179.94 seconds. Although the final optimality gap of 78.5% is substantial, it is a reasonable outcome given the unprecedented scale of this problem, representing the largest SCLA instance with queue congestion to date.

Figure 2 shows the stations selected in the best solution identified. Figure 2 (b) focuses on TAZ-based stations (squares) that are opened in the solution. Each station symbol also indicates which charger types (slow, moderate, or fast) were installed at that location.

Several trends emerge from these figures. First, most depot stations opened in or around the city center (Figure 2 (a)), suggesting higher demands and thus a stronger incentive to co-locate chargers near major demand points. The TAZ-based stations are more widely dispersed across the metropolitan region (Figure 2 (b)). These TAZ stations host a mix of fast and moderate chargers, while depots include more slow chargers. This pattern appears consistent with the model’s goal of balancing high-traffic locations (which benefit from faster chargers to limit queues) with cost-effective service in lower-density areas (where slower chargers may suffice).

The solution indicates that combining depot and TAZ options provides good spatial coverage

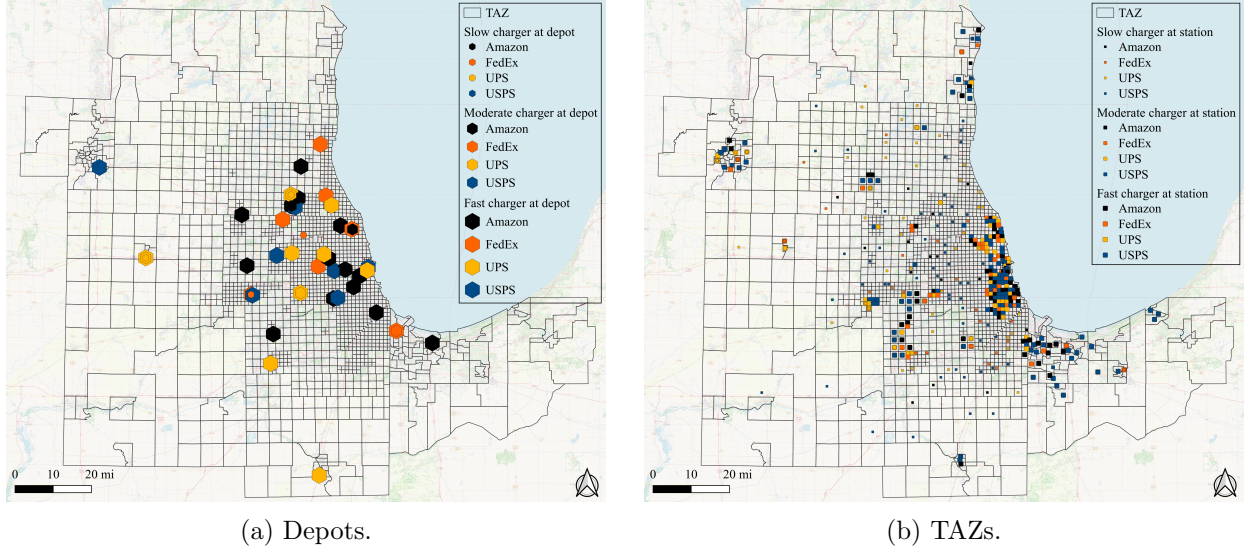


Figure 2: Spatial distribution of open depot and TAZ stations

while still adhering to budget and queue constraints. Many of the TAZ sites offering fast chargers are located near major corridors or in higher-demand neighborhoods, minimizing detour time and wait times for vehicles. Meanwhile, more modest charging installations at peripheral TAZ stations reduce congestion at busier stations without excessively increasing costs. These location and charger-type decisions reflect the model’s attempt to serve 449,367 households efficiently under multiagency operations where any household can use any open station, reinforcing that fast chargers are allocated to busier or central sites and slow or moderate chargers serve moderately traveled or outlying zones.

6.5 Sensitivity Analysis

We perform sensitivity analyses to understand how changes in key model parameters impact total costs (\mathbb{C}) across different household sizes ($|\mathcal{I}| = 50, 100, 200$). We assume a multiagency policy, meaning any open station whether at a TAZ or an existing depot can serve any household. For each parameter configuration and household size we generate five random instances; the average results are presented in [Figure 3](#). The analysis focuses on four main parameters: station costs (C^ϕ), waiting time costs (C^τ), charger costs (C^ξ), and charger powers ($P_k \forall k \in \mathcal{K}$). [Figure 3\(a\)](#) shows that station costs (C^ϕ) have the most pronounced influence on \mathbb{C} , especially for scenarios with fewer households. For instance, a 100% increase in C^ϕ leads to cost escalations of approximately 52.20% to 65.62%, with $|\mathcal{I}| = 50$ displaying the greatest sensitivity. This indicates that infrastructure-related expenses disproportionately affect smaller sets of households. In contrast, [Figure 3\(b\)](#) demonstrates that waiting time costs (C^τ) have a nonlinear and increasingly significant impact as the number of households grows. A 10% increase in C^τ raises total costs by approximately 18.83% to 22.82%. Larger $|\mathcal{I}|$ values amplify this effect since more households imply higher EV arrival rates and more frequent charging events, thereby magnifying the consequences of driver idle time. Reductions in charger costs (C^ξ) show a more uniform effect across different household sizes ([Figure 3\(c\)](#)). An 80% decrease in C^ξ leads to roughly 14–15% total cost savings, irrespective of $|\mathcal{I}|$. This uniformity suggests that cost-effective charging equipment investments benefit last-mile delivery operations across all scales. Improvements in charger powers (P_k) yield more modest, yet scale-dependent benefits ([Figure 3\(d\)](#)). Doubling P_k results in cost reductions of about 1.41%, 2.14%, and 3.17%

for $|\mathcal{I}| = 50, 100$, and 200 , respectively. Thus, while enhanced charging speeds consistently reduce total costs, their impact grows as the number of households (and, consequently, station utilization) increases.

As a whole, these results highlight the interdependence between infrastructure costs, operational factors, and charging technology in shaping the economics of last-mile EV delivery. Although station costs dominate when household counts are low, waiting time and charger performance considerations become increasingly critical as the delivery network expands. Therefore we believe that strategic decision-making should balance fixed infrastructure investments with enhancements in charging operations and technology, ensuring better performance across varying population sizes.

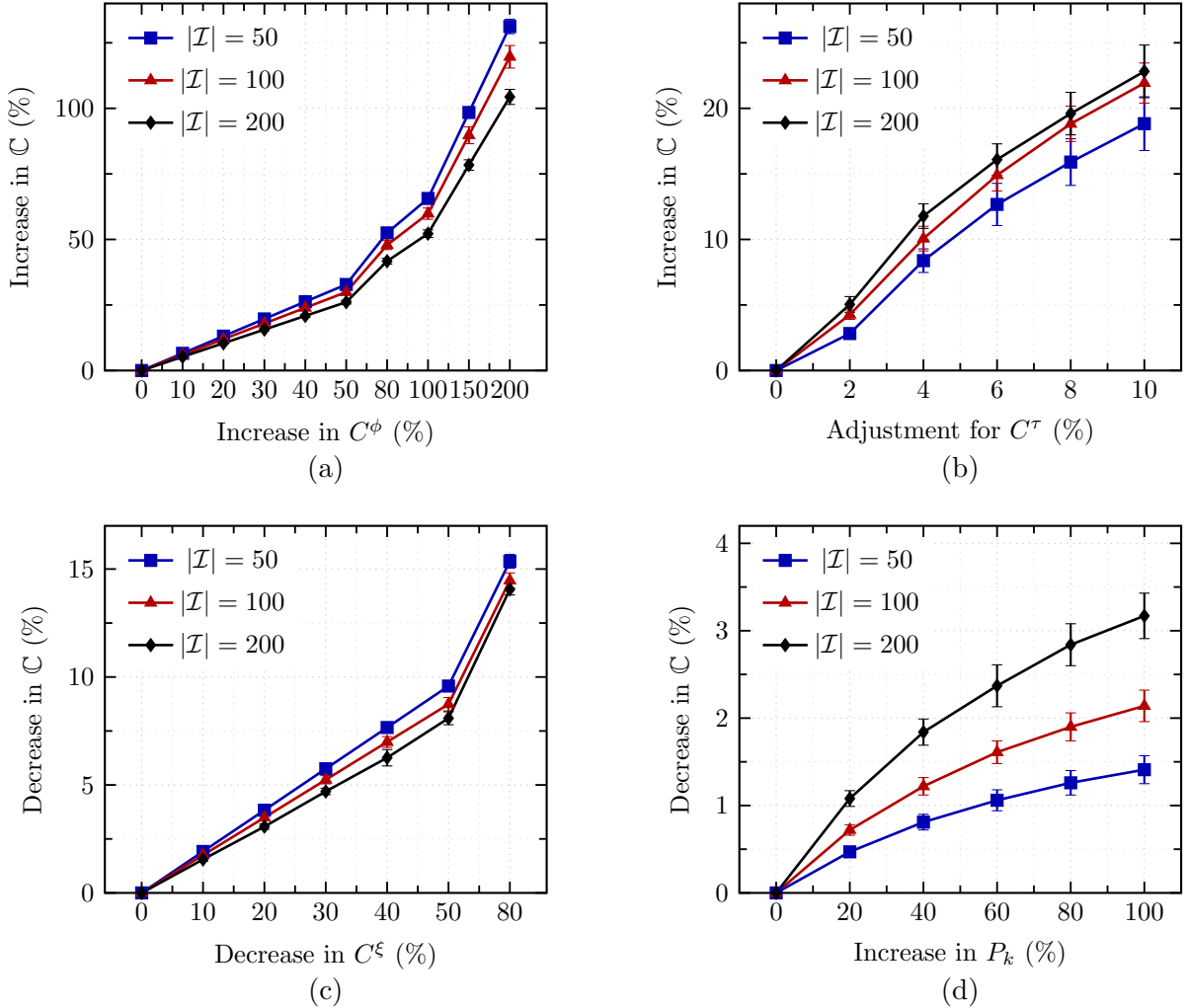


Figure 3: Sensitivity analysis of changes in \mathbb{C} under various parameter adjustments.

7 Conclusion

Our paper presents a fresh approach to charging infrastructure planning by modeling the EV charging station location problem as a stochastic location model with congestion and immobile servers (SLCIS), which we refer to as the stochastic charger location and allocation problem (SCLA). We formulate the problem as a mixed-integer quadratic program and present two exact formulations,

although the model building becomes computationally prohibitive for large scales using the exact methods. To address this issue, we have developed a Lagrangian-based dual decomposition framework, decomposing the problem into station-level subproblems, and we present two formulations for their solution. We use high-performance parallel computing across multiple partitions and solve the subproblems in parallel via a semi-relaxation and cutting-plane approach. We employed a three-step rounding heuristic to get integral solutions and used a subgradient method to improve lower bounds. Our extensive computational study on Chicago metropolitan data demonstrates that this framework consistently produces high-quality solutions for extremely large instances, whereas exact formulations cannot even be built. In practice, multiagency collaboration with combined depot and TAZ installations can yield substantial cost savings and reduced congestion. In conclusion, our paper yields valuable insights for strategic EV charging infrastructure planning. Our large-scale SCLA solution methodology proves highly effective in solving complex charging network design problems. It offers a tool for optimizers, urban planners, and policymakers navigating the transition to electric vehicle infrastructure.

Future research directions may include incorporating time-varying demand patterns, exploring diverse geographic distributions of potential locations, and assessing the impact of emerging EV charger technologies on optimal network design. One could also refine our subgradient updates with more advanced techniques, such as proximal or bundle methods, to further accelerate convergence and tighten dual bounds. As we advance toward sustainable urban mobility, our paper provides a tool for informed decision-making in EV charging infrastructure development in the United States.

Acknowledgment

This material is based upon work supported by the U.S. Department of Energy, Office of Science, under contract number DE-AC02-06CH11357. This report and the work described were sponsored by the U.S. Department of Energy (DOE) Vehicle Technologies Office (VTO) under the Systems and Modeling for Accelerated Research in Transportation (SMART) Mobility Laboratory Consortium, an initiative of the Energy Efficient Mobility Systems (EEMS) Program. Erin Boyd, a DOE Office of Energy Efficiency and Renewable Energy (EERE) manager, played an important role in establishing the project concept, advancing implementation, and providing guidance. The authors remain responsible for all findings and opinions presented in the paper. The findings are not suggestions for agencies to implement given the assumptions made in this study.

Computations for this research were performed on the Pennsylvania State University's Institute for Computational and Data Sciences' Roar supercomputer.

References

- Aboolian R, Aboolian R, Berman O, Berman O, Drezner Z, Drezner Z, 2009 *The multiple server center location problem*. *Annals of Operations Research* URL <http://dx.doi.org/10.1007/s10479-008-0341-2>.
- Aboolian R, Berman O, Drezner Z, 2008 *Location and allocation of service units on a congested network*. *IIE Transactions* 40(4):422–433, URL <http://dx.doi.org/10.1080/07408170701411385>.
- Aboolian R, Elhedhli S, Karimi M, 2022 *An efficient approach for service system design with immobile servers, stochastic demand, congestion, and consumer choice*. *Journal of Supply Chain and Operations Management* 20(1):1.
- Ahmadi-Javid A, Berman O, Hoseinpour P, 2018 *Location and capacity planning of facilities with general service-time distributions using conic optimization*. *arXiv preprint arXiv:1809.00080* .
- Ahmadi-Javid A, Hoseinpour P, 2022 *Convexification of queueing formulas by mixed-integer second-order cone programming: An application to a discrete location problem with congestion*. *INFORMS Journal on Computing* 34(5):2621–2633, URL <http://dx.doi.org/10.1287/ijoc.2021.1125>.
- Ahmadi-Javid A, Ramshe N, 2020 *Linear formulations and valid inequalities for a classic location problem with congestion: a robust optimization application*. *Optimization Letters* 14(5):1265–1285, URL <http://dx.doi.org/10.1007/s11590-019-01419-8>.
- Amiri A, 1997 *Solution procedures for the service system design problem*. *Computers & Operations Research* 24(1):49–60, URL [http://dx.doi.org/10.1016/S0305-0548\(96\)00022-6](http://dx.doi.org/10.1016/S0305-0548(96)00022-6).
- Auld J, Hope M, Ley H, Sokolov V, Xu B, Zhang K, 2016 *POLARIS: Agent-based modeling framework development and implementation for integrated travel demand and network and operations simulations*. *Transportation Research Part C: Emerging Technologies* 64:101–116, URL <http://dx.doi.org/10.1016/j.trc.2015.07.017>.
- Barahona F, Anbil R, 2000 *The volume algorithm: Producing primal solutions with a subgradient method*. *Mathematical Programming* 87:385–399.
- Barahona F, Chudak FA, 2005 *Near-optimal solutions to large-scale facility location problems*. *Discrete Optimization* 2(1):35–50.
- Bennett J, Mishra P, Miller E, Borlaug B, Meintz A, Birky A, 2022 *Estimating the breakeven cost of delivered electricity to charge class 8 electric tractors*. Technical report, National Renewable Energy Lab.(NREL), Golden, CO (United States).
- Berman O, Drezner Z, 2007 *The multiple server location problem*. *Journal of the Operational Research Society* 58(1):91–99, URL <http://dx.doi.org/10.1057/palgrave.jors.2602126>.
- Berman O, Krass D, 2019 *Stochastic location models with congestion*. Laporte G, Nickel S, Saldanha da Gama F, eds., *Location Science*, chapter 17, 477–531 (Switzerland: Springer), 2nd edition, ISBN 978-3-030-32176-5.
- Borst S, Mandelbaum A, Reiman MI, 2004 *Dimensioning large call centers*. *Operations Research* 52(1):17–34, URL <http://dx.doi.org/10.1287/opre.1030.0081>.
- Boyd S, Xiao L, Mutapcic A, 2003 *Subgradient methods*. lecture notes of EE392o, Stanford University, Autumn Quarter 2004(01).
- Castillo I, Ingolfsson A, Sim T, 2009 *Social optimal location of facilities with fixed servers, stochastic demand, and congestion*. *Production and Operations Management* 18(6):721–736, URL <http://dx.doi.org/10.1111/j.1937-5956.2009.01045.x>.
- Chen R, Qian X, Miao L, Ukkusuri SV, 2020 *Optimal charging facility location and capacity for electric vehicles considering route choice and charging time equilibrium*. *Computers & Operations Research* 113:104776, URL <http://dx.doi.org/10.1016/j.cor.2019.104776>.
- Cokyasar T, Jin M, 2023 *Additive manufacturing capacity allocation problem over a network*. *IIE Transactions* 55(8):807–820, URL <http://dx.doi.org/10.1080/24725854.2022.2120222>.
- Cui Q, Weng Y, Tan CW, 2019 *Electric vehicle charging station placement method for urban areas*. *IEEE Transactions on Smart Grid* 10(6):6552–6565, URL <http://dx.doi.org/10.1109/TSG.2019.2907262>.

- Dalcín L, Paz R, Storti M, D'Elía J, 2008 *MPI for Python: Performance improvements and MPI-2 extensions*. *Journal of Parallel and Distributed Computing* 68(5):655–662.
- Davatgari A, 2021 *Location planning for electric charging stations and wireless facilities in the era of autonomous vehicle operations*. Master's thesis, Purdue University.
- Davatgari A, Cokyasar T, Subramanyam A, Larson J, Mohammadian AK, 2024 *Electric vehicle supply equipment location and capacity allocation for fixed-route networks*. *European Journal of Operational Research* 317(3):953–966, URL <http://dx.doi.org/10.1016/j.ejor.2024.04.022>.
- Davidov S, Pantoš M, 2017 *Stochastic expansion planning of the electric-drive vehicle charging infrastructure*. *Energy* 141:189–201, URL <http://dx.doi.org/10.1016/j.energy.2017.09.065>.
- Dolsak N, Prakash A, 2021 *The lack of EV charging stations could limit EV growth*. *Forbes* URL <https://www.forbes.com/sites/prakashdolsak/2021/05/05/the-lack-of-ev-charging-stations-could-limit-ev-growth/>, accessed on July 31, 2024.
- Electrify America, 2024 *Pricing and plans for EV charging*. <https://www.electrifyamerica.com/pricing/>, accessed: 2024-08-13.
- Elhedhli S, 2006 *Service system design with immobile servers, stochastic demand, and congestion*. *Manufacturing & Service Operations Management* 8(1):92–97, URL <http://dx.doi.org/10.1287/msom.1050.0094>.
- Elhedhli S, Elhedhli S, Wang Y, Wang Y, Saif A, Saif A, 2018 *Service system design with immobile servers, stochastic demand and concave-cost capacity selection*. *Computers & Operations Research* URL <http://dx.doi.org/10.1016/j.cor.2018.01.019>.
- Erdoğan S, Çapar İ, Çapar İ, Nejad MM, 2022 *Establishing a statewide electric vehicle charging station network in Maryland: A corridor-based station location problem*. *Socio-Economic Planning Sciences* 79:101127, URL <http://dx.doi.org/10.1016/j.seps.2021.101127>.
- Etebari F, 2019 *A column generation algorithm for the choice-based congested location-pricing problem*. *Computers & Industrial Engineering* URL <http://dx.doi.org/10.1016/j.cie.2019.03.023>.
- FareEye, 2024 *Electric vehicles for last mile delivery: Future, benefits & challenges*. <https://fareye.com/resources/blogs/electric-vehicles-for-last-mile-delivery>, accessed: January 2024.
- FedEx, 2024a *FedEx company structure*. <https://www.fedex.com/en-us/about/company-structure.html>, data on annual revenue, accessed on: 13 August 2024.
- FedEx, 2024b *FedEx company structure*. <https://www.fedex.com/en-us/about/company-structure.html>, data on operational days per year, accessed on: 13 August 2024.
- FedEx, 2024c *FedEx company structure*. <https://www.fedex.com/en-us/about/company-structure.html>, data on fleet size, accessed on: 13 August 2024.
- FedEx, 2024d *FedEx company structure*. <https://www.fedex.com/en-us/about/company-structure.html>, data on daily packages delivered, accessed on: 13 August 2024.
- FedEx Express, 2023 *Fedex deploys electric vehicles to advance sustainability goal of zero-emissions last-mile delivery in India*. <https://newsroom.fedex.com/newsroom/middle-east-indian-subcontinent-and-africa/fedex-deploys-electric-vehicles-to-advance-sustainability-goal-of-zero-emissions-last-mile-deliver> press Release.
- Glover F, Laguna M, 1998 *Tabu Search* (Springer).
- Grassmann W, 1983 *The convexity of the mean queue size of the M/M/c queue with respect to the traffic intensity*. *Journal of Applied Probability* 20(4):916–919, URL <http://dx.doi.org/10.2307/3213605>.
- Guignard M, 2003 *Lagrangian relaxation*. *Top* 11:151–200.
- Gurobi Optimization, LLC, 2024 *Gurobi optimizer reference manual*. Online, URL <https://www.gurobi.com>.
- Góez JC, Góez JC, Anjos MF, Anjos MF, 2017 *Second-order cone optimization formulations for service system design problems with congestion*. null URL http://dx.doi.org/10.1007/978-3-030-12119-8_5.
- Hale TS, Moberg CR, 2003 *Location science research: A review*. *Annals of Operations Research* 123:21–35, URL <http://dx.doi.org/10.1023/A:1026110926707>.

- Halfin S, Whitt W, 1981 *Heavy-traffic limits for queues with many exponential servers*. *Operations Research* 29(3):567–588, URL <http://dx.doi.org/10.1287/opre.29.3.567>.
- International Energy Agency, 2024 *Global EV outlook 2024*. URL <https://www.iea.org/reports/global-ev-outlook-2024>, licence: CC BY 4.0.
- Jordán J, Palanca J, Martí P, Julian V, 2022 *Electric vehicle charging stations emplacement using genetic algorithms and agent-based simulation*. *Expert Systems with Applications* 197:116739, URL <http://dx.doi.org/10.1016/j.eswa.2022.116739>.
- Kchaou-Boujelben M, 2021 *Charging station location problem: A comprehensive review on models and solution approaches*. *Transportation Research Part C: Emerging Technologies* 132:103376, URL <http://dx.doi.org/10.1016/j.trc.2021.103376>.
- Kelley JE Jr, 1960 *The cutting-plane method for solving convex programs*. *Journal of the society for Industrial and Applied Mathematics* 8(4):703–712.
- Lee HL, Cohen MA, 1983 *A note on the convexity of performance measures of M/M/c queueing systems*. *Journal of Applied Probability* 20(4):920–923, URL <http://dx.doi.org/10.2307/3213606>.
- Lightning eMotors, 2022 *Lightning electric class 6 lowcab forward*. <https://lightningemotors.com/>, accessed on: 03 August 2024.
- Liu H, Wang DZ, 2017 *Locating multiple types of charging facilities for battery electric vehicles*. *Transportation Research Part B: Methodological* 103:30–55, URL <http://dx.doi.org/10.1016/j.trb.2017.01.005>.
- Luo X, Qiu R, 2020 *Electric vehicle charging station location towards sustainable cities*. *International Journal of Environmental Research and Public Health* 17(8):2785, URL <http://dx.doi.org/10.3390/ijerph17082785>.
- McCormick GP, 1976 *Computability of global solutions to factorable nonconvex programs: Part I—convex underestimating problems*. *Mathematical Programming* 10(1):147–175.
- Rivian EDV, 2024 *Rivian EDV*. https://en.wikipedia.org/wiki/Rivian_EDV, specific section on battery capacity referenced, accessed on: 13 August 2024.
- Smith M, Castellano J, 2015 *Costs associated with non-residential electric vehicle supply equipment*. Technical report, U.S. Department of Energy, URL https://afdc.energy.gov/files/u/publication/evse_cost_report_2015.pdf, accessed on: 13 August 2024.
- Stewart WJ, 2009 *Probability, Markov Chains, Queues, and Simulation: The Mathematical Basis of Performance Modeling* (Princeton University Press).
- Syam SS, 2008 *A multiple server location-allocation model for service system design*. *Computers & Operations Research* URL <http://dx.doi.org/10.1016/j.cor.2006.10.019>.
- Upper Inc, 2024 *UPS driver salary*. <https://www.upperinc.com/blog/ups-driver-salary>, specific section on average hourly wage after four years referenced, accessed on: 13 August 2024.
- Vidarthi N, Jayaswal S, 2014 *Efficient solution of a class of location-allocation problems with stochastic demand and congestion*. *Computers & Operations Research* 48:20–30, URL <http://dx.doi.org/10.1016/j.cor.2014.02.014>.
- Vidarthi N, Vidarthi N, Kuzgunkaya O, Kuzgunkaya O, 2015 *The impact of directed choice on the design of preventive healthcare facility network under congestion*. *Health Care Management Science* URL <http://dx.doi.org/10.1007/s10729-014-9274-2>.
- Wang Q, Batta R, Rump CM, 2002 *Algorithms for a facility location problem with stochastic customer demand and immobile servers*. *Annals of Operations Research* 111:17–34.
- Williams K, 2020 *How many hours can a truck driver drive?* <https://www.cdljobs.com/news-notes/news/how-many-hours-can-a-truck-driver-drive>, accessed on: 13 August 2024.
- Wood E, Borlaug B, Moniot M, Lee DYD, Ge Y, Yang F, Liu Z, 2023 *The 2030 national charging network: Estimating US light-duty demand for electric vehicle charging infrastructure*. Technical report, National Renewable Energy Laboratory (NREL), Golden, CO (United States).
- Xi X, Sioshansi R, Marano V, 2013 *Simulation-optimization model for location of a public electric vehicle charging infrastructure*. *Transportation Research Part D: Transport and Environment* 22:60–69, URL <http://dx.doi.org/10.1016/j.trd.2013.02.014>.

Yilmaz M, Krein PT, 2012 *Review of battery charger topologies, charging power levels, and infrastructure for plug-in electric and hybrid vehicles. IEEE Transactions on Power Electronics* 28(5):2151–2169, URL <http://dx.doi.org/10.1109/TPEL.2012.2212917>.

Appendix

Algorithm 1 Construction of \mathcal{J}_i and \mathcal{I}_j

Input: \mathcal{I} : set of households; \mathcal{J} : set of candidate stations; k_c : number of nearest stations to consider; $\mathbf{x}(i)$: (latitude, longitude) for each household $i \in \mathcal{I}$; $\mathbf{x}(j)$: (latitude, longitude) for each station $j \in \mathcal{J}$.

Output: \mathcal{J}_i : up to k_c closest stations for each i ; \mathcal{I}_j : set of households for which j is among their k_c closest.

```

1: Build a 2D  $k$ -d tree from the station coordinates  $\mathbf{x}(j)$ ,  $j \in \mathcal{J}$ .
2: for  $i \in \mathcal{I}$  do
3:   Query the  $k_c$  nearest stations to  $\mathbf{x}(i)$  using the  $k$ -d tree.
4:    $\mathcal{J}_i(i) \leftarrow$  those  $k_c$  stations
5: end for
6: for  $j \in \mathcal{J}$  do
7:    $\mathcal{I}_j(j) \leftarrow \{i \in \mathcal{I} \mid j \in \mathcal{J}_i(i)\}$ 
8: end for
9: return  $\mathcal{J}_i, \mathcal{I}_j$ 

```

Algorithm 2 Station Opening

Input: \mathcal{J} : set of potential station locations, \mathcal{I} : set of all households, y_j^t for all $j \in \mathcal{J}$: station open states at iteration t , \mathcal{I}_j for all $j \in \mathcal{J}$: set of households coverable by station j

Output: y_j' : updated station open states, \mathcal{U}^c : set of uncovered households after updating station states

```

1: Initialize  $y_j' \leftarrow y_j^t$  for all  $j \in \mathcal{J}$                                 ▷ Initialize station states
2:  $O \leftarrow \{j \in \mathcal{J} \mid y_j^t = 1\}$                                     ▷ Set of open stations
3:  $C \leftarrow \bigcup_{j \in O} \mathcal{I}_j$                                         ▷ Set of covered households
4:  $\mathcal{U}^c \leftarrow \mathcal{I} \setminus C$                                         ▷ Set of uncovered households
5: if  $\mathcal{U}^c = \emptyset$  then
6:   return  $y_j', \emptyset$                                             ▷ All households are covered; no new openings required
7: end if
8: while  $\mathcal{U}^c \neq \emptyset$  and  $\mathcal{J} \setminus O \neq \emptyset$  do
9:   For each  $j \in \mathcal{J} \setminus O$ , compute  $w_j \leftarrow |\mathcal{I}_j \cap \mathcal{U}^c|$     ▷ Compute weights
10:   $\mathcal{J}_{\text{cand}} \leftarrow \{j \in \mathcal{J} \setminus O \mid w_j > 0\}$                 ▷ Candidate stations
11:  if  $\mathcal{J}_{\text{cand}} = \emptyset$  then
12:    break                                                        ▷ No more stations can cover remaining households
13:  end if
14:   $W \leftarrow \sum_{j \in \mathcal{J}_{\text{cand}}} w_j$                                 ▷ Total weight for probability calculation
15:  For each  $j \in \mathcal{J}_{\text{cand}}$ , compute  $p_j \leftarrow w_j/W$                 ▷ Calculate selection probabilities
16:  Randomly select station  $j^*$  from  $\mathcal{J}_{\text{cand}}$  based on probabilities  $p_j$   ▷ Select station probabilistically
17:  Set  $y_{j^*}' \leftarrow 1$                                         ▷ Open station  $j^*$ 
18:  Update  $O \leftarrow O \cup \{j^*\}$                                 ▷ Update set of open stations
19:  Update  $\mathcal{U}^c \leftarrow \mathcal{U}^c \setminus \mathcal{I}_{j^*}$                             ▷ Remove covered households
20: end while
21: if  $\mathcal{U}^c = \emptyset$  then
22:   return  $y_j', \emptyset$                                         ▷ Coverage achieved for all households
23: end if

```

Algorithm 3 Household Assignment Iteration

Input: Sets $\mathcal{I}, \mathcal{J}, \mathcal{K}$; parameters $x_{ijk}^t, y_j^t, \lambda_i, \mu_k, \epsilon, \bar{S}_{jk}, EW, \mathcal{J}_i$

Output: Updated variables $x'_{ijk}, s'_{jk}, W'_{jk}, y'_j$; set of unassigned households \mathcal{U}^a

```
1: Initialize  $x'_{ijk} \leftarrow 0$  for all  $i, j, k$ 
2:  $s'_{jk} \leftarrow s_{jk}^t, W'_{jk} \leftarrow W_{jk}^t$ 
3: Compute  $D_{jk} \leftarrow \sum_{i' \in \mathcal{I}} \lambda_{i'} x_{i'jk}^t$  for all  $j, k$ 
4: Initialize  $\mathcal{U}^a \leftarrow \emptyset$ 
5: Sort  $\mathcal{I}$  in descending order of  $\lambda_i$ 
6: for each  $i \in \mathcal{I}$  do
7:    $V_i \leftarrow \{j \in \mathcal{J} : y_j^t = 1\}$ 
8:   if  $V_i = \emptyset$  then
9:      $\mathcal{U}^a \leftarrow \mathcal{U}^a \cup \{i\}$ 
10:    continue
11:   end if
12:    $\mathcal{C}_i \leftarrow \{(j, k) : j \in V_i, k \in \mathcal{K}\}$ 
13:   Sort  $\mathcal{C}_i$  by (1) descending  $x_{ijk}^t$ , (2) ascending  $C_k^\xi$ , (3) ascending  $W_{jk}$  ▷ Break ties at random
14:    $assigned \leftarrow \text{false}$ 
15:   for each  $(j, k) \in \mathcal{C}_i$  do
16:      $assigned \leftarrow \text{CHECKANDASSIGN}(i, j, k, \lambda_i, \mu_k, \epsilon, \bar{S}_{jk}, EW, D_{jk}, s'_{jk}, W'_{jk})$ 
17:     if  $assigned = \text{true}$  then
18:       break ▷ Move to next household
19:     end if
20:   end for
21:   if  $assigned = \text{false}$  then
22:      $\mathcal{U}^a \leftarrow \mathcal{U}^a \cup \{i\}$ 
23:   end if
24: end for
25: for each  $j \in \mathcal{J}$  do
26:    $y'_j \leftarrow 1$  if  $\exists i, k : x'_{ijk} = 1$ , else  $y'_j \leftarrow 0$ 
27: end for
28: return  $x'_{ijk}, s'_{jk}, W'_{jk}, y'_j, \mathcal{U}^a$ 
```

Algorithm 4 Check and Assign Feasibility

Input: Household i , station j , charger type k , parameters $\lambda_i, \mu_k, \epsilon, \bar{S}_{jk}, EW$, and current values

$$D_{jk}, s'_{jk}, W'_{jk}$$

Output: Returns **true** if assignment is successful, else **false**. Updates $x'_{ijk}, s'_{jk}, W'_{jk}$ on success.

```
1:  $D_{jk}^c \leftarrow D_{jk} + \lambda_i$ 
2:  $s_{jk}^{\text{req}} \leftarrow \lceil \frac{D_{jk}^c}{\mu_k(1-\epsilon)} \rceil$ 
3: if  $s_{jk}^{\text{req}} > \bar{S}_{jk}$  then
4:   return false ▷ Capacity constraint violated
5: end if
6:  $s_{jk}^c \leftarrow \max(s'_{jk}, s_{jk}^{\text{req}})$ 
7: while  $s_{jk}^c \leq \bar{S}_{jk}$  do
8:    $\rho_{jk}^c \leftarrow \frac{D_{jk}^c}{s_{jk}^c \mu_k}$ 
9:   if  $\rho_{jk}^c \geq 1$  then
10:    break ▷ Cannot assign with current  $s_{jk}^c$ 
11:  end if
12:   $W_{jk}^c \leftarrow \mathbb{W}(\rho_{jk}^c, s_{jk}^c, \mu_k)$ 
13:  if  $W_{jk}^c \leq EW + \frac{1}{\mu_k}$  then
14:     $D_{jk} \leftarrow D_{jk}^c$ 
15:     $s'_{jk} \leftarrow s_{jk}^c$ 
16:     $x'_{ijk} \leftarrow 1$ 
17:     $W'_{jk} \leftarrow W_{jk}^c$ 
18:    return true
19:  else
20:     $s_{jk}^c \leftarrow s_{jk}^c + 1$ 
21:  end if
22: end while
23: return false ▷ No feasible assignment found
```

Algorithm 5 Calculate Additional Stations for Overload

Input: Unassigned households \mathcal{U}^a ; current depot states y'_j ; depot accessibility \mathcal{J}_i ; household assignments

$$\mathcal{I}_j$$

Output: Updated depot states y'_j

```
1:  $\mathcal{C} \leftarrow \bigcup_{i \in \mathcal{U}^a} \mathcal{J}_i$  ▷ Candidate depots accessible to unassigned households
2:  $\mathcal{C} \leftarrow \mathcal{C} \setminus \{j \in \mathcal{J} \mid y'_j = 1\}$  ▷ Exclude already open depots
3: if  $\mathcal{C} = \emptyset$  then
4:   return  $y'_j$  ▷ No additional depots can be opened
5: end if
6: For each  $j \in \mathcal{C}$ , compute  $w_j \leftarrow |\mathcal{I}_j \cap \mathcal{U}^a|$ 
7:  $j^* \leftarrow \arg \max_{j \in \mathcal{C}} w_j$  ▷ Depot covering most unassigned households
8:  $y'_{j^*} \leftarrow 1$  ▷ Open depot  $j^*$ 
9: return  $y'_j$ 
```

Algorithm 6 Primal Feasible Solution Heuristic

Input: Sets $\mathcal{I}, \mathcal{J}, \mathcal{K}$; variables x_{ijk}^t, y_j^t ; parameters $\lambda_i, \mu_k, \epsilon, \bar{S}_{jk}, EW, \mathcal{J}_i, \mathcal{I}_j$

Output: Feasible assignment x'_{ijk} , updated depot states y'_j , charger allocations s'_{jk} , waiting times W'_{jk}

```
1: Call Algorithm 2 with  $\mathcal{J}, \mathcal{I}, y_j^t, \mathcal{I}_j$  to obtain  $y'_j$  and  $\mathcal{U}^c$ 
2: if  $\mathcal{U}^c = \emptyset$  then
3:   Initialize  $\mathcal{U}^a \leftarrow \emptyset$ 
4:   while  $\mathcal{U}^a \neq \emptyset$  do
5:      $(x'_{ijk}, s'_{jk}, W'_{jk}, y'_j, \mathcal{U}^a) \leftarrow$ 
6:       HOUSEHOLDASSIGNMENTITERATION( $\mathcal{I}, \mathcal{J}, \mathcal{K}, x_{ijk}^t, y_j^t, \lambda_i, \mu_k, \epsilon, \bar{S}_{jk}, EW, \mathcal{J}_i$ )
7:     if  $\mathcal{U}^a \neq \emptyset$  then
8:       Call Algorithm 5 with  $\mathcal{U}^a, y'_j, \mathcal{J}_i$  to update  $y'_j$ 
9:     end if
10:  end while
11:  return  $x'_{ijk}, y'_j, s'_{jk}, W'_{jk}$ 
12: else
13:  return Failure
14: end if
```

The submitted manuscript has been created by UChicago Argonne, LLC, Operator of Argonne National Laboratory (“Argonne”). Argonne, a U.S. Department of Energy Office of Science laboratory, is operated under Contract No. DE-AC02-06CH11357. The U.S. Government retains for itself, and others acting on its behalf, a paid-up nonexclusive, irrevocable worldwide license in said article to reproduce, prepare derivative works, distribute copies to the public, and perform publicly and display publicly, by or on behalf of the Government. The Department of Energy will provide public access to these results of federally sponsored research in accordance with the DOE Public Access Plan <http://energy.gov/downloads/doe-public-access-plan>.